IMAGE-BASED TIP FORCE ESTIMATION ON STEERABLE INTRACARDIAC CATHETERS USING LEARNING-BASED METHODS

Hamid Reza Nourani Nezhad

A thesis

in

The Department

of

Mechanical, Industrial, and Aerospace Engineering

Presented in Partial Fulfillment of the Requirements

For the Degree of Master of Applied Science in Mechanical Engineering

Concordia University

Montréal, Québec, Canada

April 2021

Concordia University

School of Graduate Studies

This is to certify that the thesis prepared

By: **Hamid Reza Nourani Nezhad**

Entitled: **Image-based Tip Force Estimation on Steerable Intracardiac Catheters Using Learning-based Methods**

and submitted in partial fulfillment of the requirements for the degree of

Master of Applied Science in Mechanical Engineering

complies with the regulations of this University and meets the accepted standards with respect to originality and quality.

Signed by the final examining commitee:

Dr. Mojtaba Kheiri _____ Chair

Dr. Farnoosh Naderkhani _____ External Examiner

Dr. Mojtaba Kheiri _____ Examiner

Dr. Javad Dargahi _____ Supervisor

Approved by Dr. Sivakumar Narayanswamy _____
Graduate Program Director

Date of Defence: April 8, 2021

Dr. Mourad Debbabi, Interim Dean

Gina Cody School of Engineering and Computer Science

Abstract

Image-based Tip Force Estimation on Steerable Intracardiac Catheters Using Learning-based Methods

Hamid Reza Nourani Nezhad

Minimally invasive surgery has turned into the most commonly used approach to treat cardiovascular diseases during the surgical procedure; it is hypothesized that the absence of haptic (tactile) feedback and force presented to surgeons is a restricting factor. The use of ablation catheters with the integrated sensor at the tip results in high cost and noise complications. In this thesis, two sensor-less methods are proposed to estimate the force at the intracardiac catheter's tip. Force estimation at the catheter tip is of great importance because insufficient force in ablation treatment may result in incomplete treatment and excessive force leads to damaging the heart chamber. Besides, adding the sensor to intracardiac catheters adds complexity to their structures. This thesis is categorized into two sensor-less approaches: 1- Learning-Based Force Estimation for Intracardiac Ablation Catheters, 2- A Deep-Learning Force Estimator System for Intracardiac Catheters. The first proposed method estimates catheter-tissue contact force by learning the deflected shape of the catheter tip section image. A regression model is developed based on predictor variables of tip curvature coefficients and knob actuation. The learning-based approach achieved force predictions in close agreement with experimental contact force measurements. The second approach proposes a deep learning method to estimate the contact forces directly from the catheter's image tip. A convolutional neural network extracts the catheter's deflection through input images and translates them into the corresponding forces. The

ResNet graph was implemented as the architecture of the proposed model to perform a regression. The model can estimate catheter-tissue contact force based on the input images without utilizing any feature extraction or pre-processing. Thus, it can estimate the force value regardless of the tip displacement and deflection shape. The evaluation results show that the proposed method can elicit a robust model from the specified data set and approximate the force with appropriate accuracy.

Acknowledgments

I would like to thank my supervisor Prof. Javad Dargahi for his support during the running of this project. My warmhearted thanks to my mentor Pedram Fekri for his patience and academic advice on this work. Furthermore, I would like to thank my colleagues Amir Hooshiar, Naghme Bandari, Amir Sayadi, Mohammad Jolaie, Hamidreza Khodashenas, Saman Namvarchi, Pegah Yaftian, Sevin Samadi and Nima Amoie in the RoboSurge Lab for their suggestions, collaborative effort, and beautiful unforgettable memories they left for me while carrying this work-study.

I sincerely thank my parents Houshang, Giti, and my brother Alireza, who were a great encouragement to me from home. I dedicate this work to them for their support and unconditional love.

Warm and kind thanks to Concordia University and the staff for paving the way for me to pursue my goals and create such a friendly environment.

Contents

List of Figures **ix**

List of Tables **xii**

1 Introduction and Review: Cardiac Arrhythmia and Learning-based Methods **1**

1.1 Minimally Invasive Surgery (MIS) 1

1.1.1 Cardiovascular Intervention Procedures 2

1.2 Cardiac Arrhythmia 4

1.3 Medication and Radio Frequency Ablation 6

1.4 Artificial Intelligence 8

1.4.1 Machine Learning Technologies and Techniques 10

1.4.2 Medical Applications 11

1.5 Research Objectives 15

1.6 Contribution of the Author 15

1.7 Organization of the Thesis 16

2 Literature Review **17**

2.1 Trends in the Adoption of Robotic Surgery 17

2.2 Necessity of Estimation the Contact Force 21

2.3 Catheter-tissue Contact Force Estimation Approaches 23

2.3.1 Instrumented Cardiac Catheters (sensor-based) 23

2.3.2 Model-based Force Estimation Methods (sensor-less) 24
2.3.2.1 Multi-body Dynamics Models 24
2.3.2.2 Particle-Based Dynamics Models 25
2.3.2.3 Continuum Mechanics Models 25
2.3.2.4 Imaging, Segmentation, and Shape-Sensing 27
2.3.2.5 Curve Parameterization and Estimation of Deformation 27
2.3.2.6 Force Estimation Based on X-Ray Image Feed and Shape-Sensing 27

3 Learning-Based Force Estimation for Intracardiac Ablation Catheters 29

3.1 Introduction 29
3.1.1 Necessity of force estimation 30
3.2 Methods 35
3.2.1 Learning-based force estimation 35
3.2.2 Image-based shape extraction 36
3.2.3 Curve fitting 38
3.2.4 Learning algorithm using SVRMs 39
3.2.5 Experimental setup 44
3.3 Results 46
3.3.1 System performance and study protocol 46
3.3.2 Experimental learning-based force estimation evaluation . . . 48

4 A Deep-Learning Force Estimator System for Intracardiac Catheters 53

4.1 Introduction 53
4.2 Experimental setup and procedure 59
4.2.1 Experimental setup 59
4.2.2 Data preparation 59
4.3 Methodology 63

4.4 Evaluation and Discussion 67

5 Conclusion and Future Work **72**

5.1 Conclusion 72

5.1.1 Future Work 73

Bibliography 75

List of Figures

1 Minimally invasive surgery versus traditional surgery 2

2 (a) View of a steerable catheter, (b) cross section of the distal 4

3 X-ray exposure to an interventionist and staff in (a) regular catheterization procedure, and (b) robot-assisted cathterization procedure . . 5

4 (a): Normal heart rhythm, (b): atrial fibrillation 6

5 Radio-frequency ablation catheter in contact with the heart tissue that causes abnormal electrical pathways in atrial fibrillation (AF) 8

6 Overview diagram of machine learning algorithms. 9

7 Definition of artificial intelligence 10

8 Convolutional Neural Network (CNN) for prognosis dementia classification. 13

9 The Corpath remote robotic control console positioned within the interventional cockpit, table side-mounted robotic drive, and single use cassette (inset) used to advance interventional equipment is shown . . 18

10 (a) Remote physician console, (b) Sensei and Magellanrobot systems, and (c) catheters equipped with sheath and low profile, for navigation in smaller vessels (Courtesy of Hansen Medical Inc.) 19

12 Stereotaxis robotic magnetic navigation system and imaging system . 19

11 a: Amigo remote controller, b: amigo catheter system along with a catheter implemented into the robotic arm 20

13 a: Controlling the instruments while monitoring surgical areas and incisions, b: patient card positioned beside the patient and includes the instruments and the camera controlled by the surgeon, and c: 3D vision cart 20
14 A robotic surgery device for two-hand manipulation with integrated force feedback and 3D vision, designed and developed by researchers at DLR, Germany 22
15 Intracardiac intervention procedure 32
16 Image-based force estimation through a learning model created by deflected catheter tip shape and knob actuation data. 36
17 (a) Real catheter image, (b) Binary catheter image, (c) Location of pixels and, (d) Curve fitted to catheter's pixels. 38
18 Converting global frame coordinate to local catheter coordinate. . . . 39
19 Experimental test setup simulates catheter tip in contact with heart tissue during ablation therapy. 45
20 (a) 2 DOF heart simulator equipped with F/T transducer and artificial tissue, (b) PQRST waveform of a heart in two directions. 47
21 (a): Sample of cardiac ablation catheter insertion path from femoral access, (b): detailed pathway for ablation 48
22 Machine learning flow chart. 49
23 (a) Estimation error for unseen testing data set, (b) estimated catheter tip contact forces for unseen testing data set are compared to the real force measurements. 51
24 SVR model fitted to the observed training data set. 52
25 This diagram shows the general architecture of the proposed method. 57
26 Sample of cardiac ablation catheter insertion path from femoral access. 58
27 Experimental test setup simulates catheter tip in contact with heart tissue during ablation therapy. 60

28 2 DOF heart simulator equipped with F/T transducer and artificial tissue. 61
29 The diagram demonstrates the architecture of the DCFE, which is designed based on the Resnet graph 62
30 The diagram shows the images of the catheter captured from the designed setup. Here is a set of sample images that used to evaluate the model. 66
31 The diagram illustrates the distribution of both actual and predicted force in the x and y direction. rx and ry are the real force data while px and py are the predicted values. the plot provides the minimum, maximum, median, quartiles and outliers of the data. 69
32 The graphs depict the model performance using its estimations on 154 catheter's images from the test dataset. 70
33 Closed-Loop force control using machine learning model as feedback element. 74

List of Tables

1 The overview of the papers used deep learning approach in medical areas. 14

2 Comparison of the sensor-based and model-based force estimation methods. 35

3 Samples of normalized data set including five coefficients of fitted curve to the catheter's tip section, knob actuation angle and associated tip contact force. 49

4 Tip contact force range and regression error. 50

5 Performance of the model. Min, Max and RMSE estimation errors are tabulated. 68

Nomenclature

Abbreviation	Definition
RFA	Radio-Frequency Ablation
CVD	Cardiovascular Disease
AF	Atrial Fibrillation
AAD	Anti-arrhythmic Drugs
MIS	Minimally Invasive Surgery
MIRS	Minimally Invasive Robotic Surgery
AV	Atrioventricular nodal
DOF	Degree of Freedom
DAQ	Data Acquisition Card
3D	3 Dimensional
FEM	Finite Element Method
PCI	Percutaneous Coronary Intervention
FEA	Finite Element Analysis
MRI	Magnetic Resonance Imaging
AI	Artificial Intelligence
ML	Machine Learning
DL	Deep Learning
ANN	Artificial Neural Network
SVM	Support Vector Machines
KNN	K-nearest Neighbor
ECG	Electro-Cardiography
FTD	Frontotemporal Dementia
CN	Cognitive Normal
MCI	Mild Cognitive Impairment
AD	Alzheimer's Disease

CNN	Convolutional Neural Network
RNN	Recurrent Neural Network
RBM	Restricted Boltzmann Machine
AE	Auto-Encoder
PPI	Percutaneous Peripheral Intervention
EPI	Electrophysiologic Intervention
LIM	Light Modulation Intensity
FPI	Fabry-Perot Interferometry
FBG	Fiber Bragg Grating
RGB	Red-Green-Blue
CS	Catheter Shape
Thr	Threshold
SVRM	Support Vector Regression Machines
RBF	Radial Basis Function
OH	Optimal Hyperplane
SVR	Support Vector Regression
IVC	Inferior Vena Cava
RA	Right Atrium
FO	Fossa Ovalis
PV	Pulmonary Veins
CF	Contact Force
MAE	Mean Absolute Error
C	Capacitive
PE	Piezo-electric
PR	Piezo-resistive

OPT	Optical
CM	Continuum Model
P	Particle-based
MD	Multi-body Dynamics
DG	Differential Geometry
GUI	Graphical User Interface
W	Weight Vector
b	Bias
F	Feature Space
C	Optimization Parameter
R_{emp}	Empirical Risk
KKT	Karush–Kuhn–Tucker
Avg	Average
DCFE	Deep Catheter Force Estimator
VGG	Visual Geometry Group
DNN	Dynamic Neural Network
VGG	Visual Graphics Generator
SGD	Stochastic Gradient Decent
RMSE	Root Mean Squared Error
P	Predicted Value

Chapter 1

Introduction and Review: Cardiac Arrhythmia and Learning-based Methods

1.1 Minimally Invasive Surgery (MIS)

Surgery has accomplished high-value advances in materials and micro-mechanical technology since the 1990s [1]. These achievements paved the way for producing reliable surgical instruments and robotic systems by a few minor incisions that enable a surgeon to conduct highly challenging procedures[2]. Such procedures are known as minimally invasive surgery (MIS) and laparoscopic surgery. These procedures are characterized by using a small camera and thin instruments accessing the body through small cuts or ports to perform a procedure that would typically involve more invasive direct access through a single, much larger incision (Fig. 1). Compared to open surgery, this type of surgical procedure can involve significant cost-savings because of shorter hospitalization time, reduction in blood loss, pain, and faster recovery time for the patients[3]. Minimally invasive surgery (MIS) procedures have evolved because of this wide variety of benefits. Because of the wide range of advantages

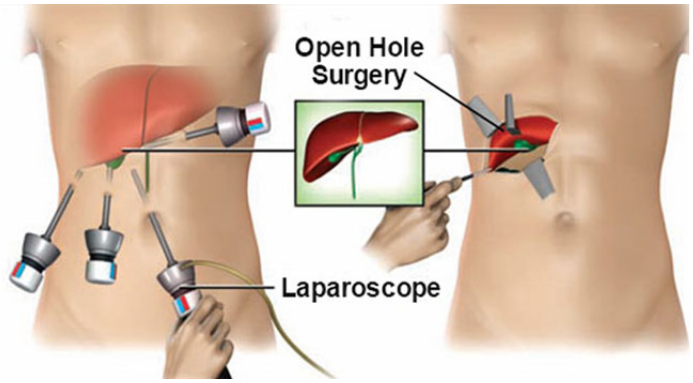

Figure 1: Minimally invasive surgery versus traditional surgery (All rights reserved by Neoalta Specialty Clinic).

in MIS, all surgical sectors, including endocrine, urological, abdominal, gynecological, general, orthopedics, and especially in cardio-thoracic, have benefited from the remarkable impact of MIS [1].

1.1.1 Cardiovascular Intervention Procedures

As mentioned, surgery treatment goes into two categories, which are known as open surgery and Minimally Invasive Surgery Therapy (MIST). Open heart surgery to treat cardiac arrhythmia began in 1968 with the initial successful division for the Wolff-Parkinson-White syndrome. Wolff-Parkinson-White is a condition causing extra electrical pathways in the heart that results in a high heartbeat rate. Following surgical procedures carried approaches such as the right and left atrial isolation procedure for atrial tachycardia, the corridor procedure, and the discrete cryosurgery of the AV node for AV nodal reentrant tachycardia. Because of great steps in treating most refractory arrhythmia by endocardial catheter techniques during the past decades, the only remaining viable surgical procedures for cardiac arrhythmia are the maze procedure for atrial fibrillation, and the Dor procedure for ischemic ventricular tachycardia [4]. Minimally invasive cardiac surgery requires making minor cuts in the right side of the chest to enter the heart under the ribs instead of going into the breastbone, as is performed in a surgical procedure. The minimal invasive cardiac procedure can

be done to treat several cardiovascular problems such as atrial fibrillation, coronary artery bypass surgery, and mitral valve repair. Minimally invasive surgical (MIS) approaches have been widely accepted and immensely influenced today's surgeries in terms of fast discharging patients, reducing costs, and patient recovery time. Long instruments are most likely used in minimally invasive surgical to navigate human small ports and vessels to reach the specific organs, and it deprives surgeons of depth perception of the surgery such as haptic, tactile, and maneuverability that they are accustomed to in conventional surgeries following that in open procedures there is a coordination between their visual and tactile abilities which could help them recognize the abnormal and normal body tissue [5].

The intra-cardiac procedure is typically conducted manually. Surgeons use the steering knob at the catheter's handle to perform hand motions such as axial, rotational, and translational on the catheter's distal shaft. Fig. 1 illustrates the manipulations produced by surgeons and catheter motions. The tendon-driven ablation catheters are used to translate knob rotation at the handle to the distal shaft's bending. By turning the knob, the catheter's tendons linked to the catheter's tip are pulled and induce changes in the distal shaft.

During minimally invasive surgeries, surgeons need to visualize the surgical procedures using X-ray fluoroscopy. The frequent use of X-ray fluoroscopy might carry permanent damages to surgeons' health in the long term [7]. Nevertheless, it necessitates the use of robotic-assisted surgery and newly emerged robotic technologies to help and release surgeons from risks of radiation exposure and high radiation-shielded garments, and the accuracy of the surgery can be guaranteed and improved (Fig. 3).

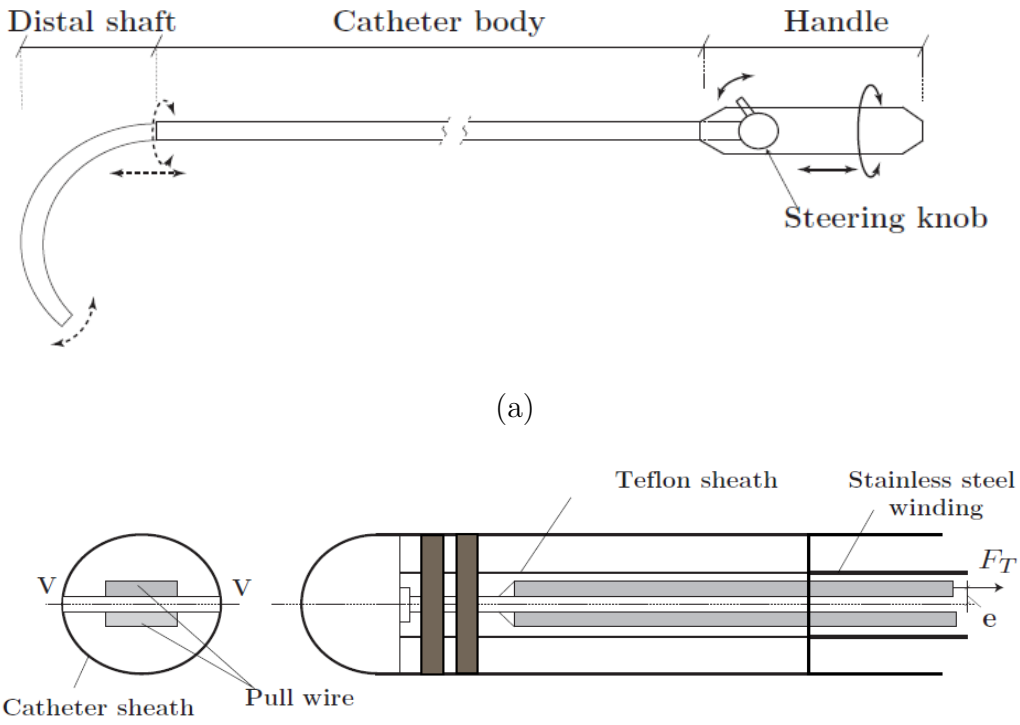

Figure 2: (a) View of a steerable catheter, (b) cross section of the distal[6].

1.2 Cardiac Arrhythmia

Where the origin of the heart motion comes from? Significant progress in understanding the origin of the heartbeat happened in 1907 when Arthur Keith and Martin Flack announced their classic marks on the sinus node. They wrote, "Our search for a well-differentiated system of fibers in the sinus, which might serve as a source for the initiation of the cardiac rhythm, has resulted in attach significance to this peculiar musculature surrounding the artery at the sino-auricular junction. It was concluded that it was within this specific cardiac muscle "that the dominating rhythm of the heart normally begins[9]. Cardiac electrical disruption leads to arrhythmias, including altered heart rates (bradyarrhythmias and tachyarrhythmias corresponding to low and high heart rates, respectively), unanticipated beats, atrial flutter,

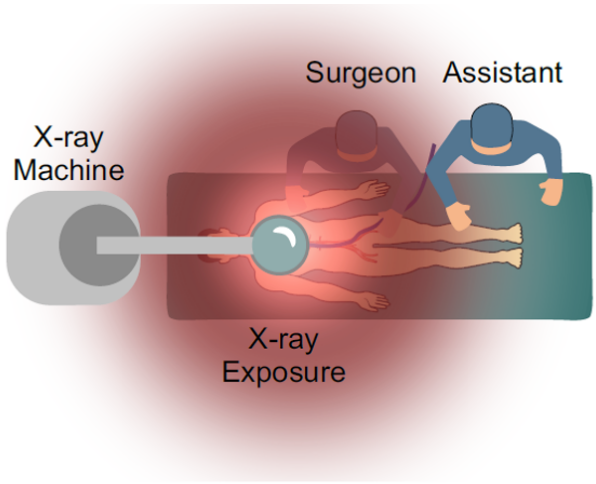

(a)

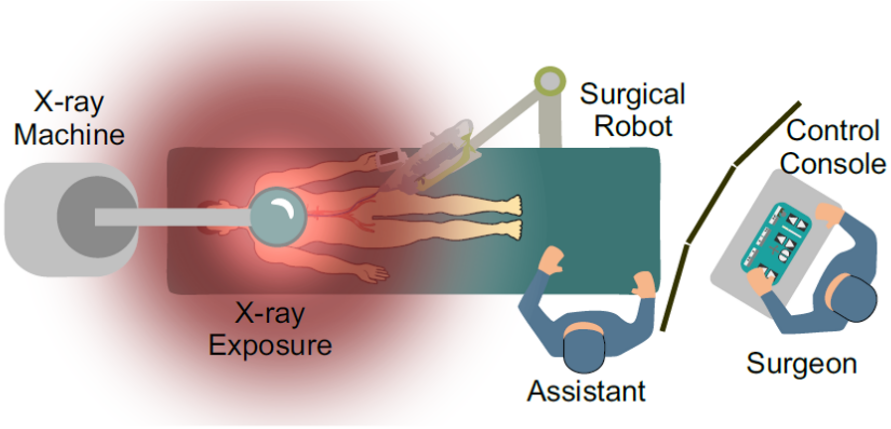

(b)

Figure 3: X-ray exposure to an interventionist and staff in (a) regular catheterization procedure, and (b) robot-assisted cathterization procedure[8].

and fibrillations, (e.g., atrial fibrillation) or ventricular[10]. Cardiovascular Conditions/Diseases (CVDs) such as Stroke, Atrial Fibrillation, Sudden Cardiac Arrest, Subclinical Atherosclerosis, Coronary Heart Disease, Heart Failure, Valvular, Venous, Aortic Diseases, and Peripheral Artery Disease are the primary reasons for death across the world, with a current estimate of 17.3 million deaths throughout the year and an anticipated rise to 23.6 million deaths by the year 2030, representing 31 percent of all global deaths[11]. Importantly, CVD risk factors promote cardiac structural differences that are frequently associated with electrical disruption and the

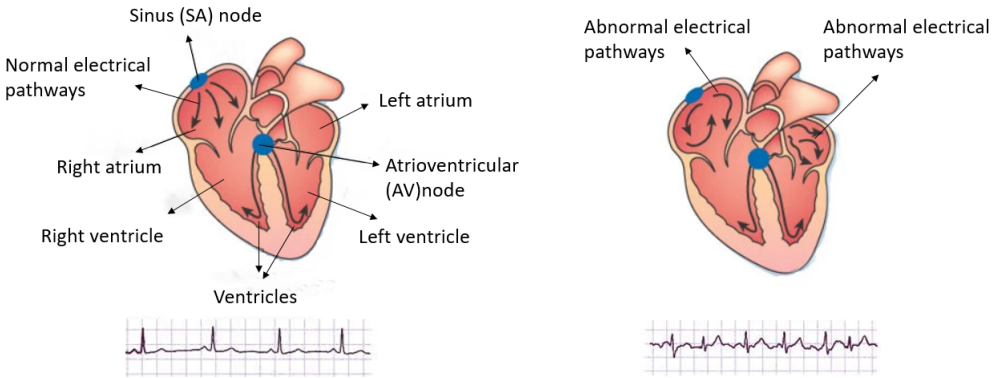

Figure 4: (a) Normal heart rhythm, (b) atrial fibrillation[14].

onset of arrhythmias[12], which account for roughly 50 percent of mortality correlated with continuous heart failure [13]. Besides, the fact that CVD may also include the impairment of the cardiac conduction system itself. Unhealthy habits like smoking, physical inactivity, nutrition, and obesity following that health factors including family history, genetics, and high blood cholesterol are the most common causes that can lead people to be afflicted with cardiovascular diseases [11].

1.3 Medication and Radio Frequency Ablation

There exists different types of treatment for arrhythmia, divided into two categories Anti-arrhythmic Drugs and RFA. Two systematic reviews have been conducted on RFA and AAD to estimate and evaluate the clinical efficiency and safety of both therapies in the treatment of atrial fibrillation (AF), Fig. 4 illustrates normal and abnormal electrical pathways that cause atrial fibrillation (AF). Therapy with antiarrhythmic drugs and anticoagulation has been considered a primary treatment in patients with symptomatic AF [15]. However, anticoagulation is suboptimal in many cases, and antiarrhythmic drugs are usually ineffective and have serious potential adverse effects[16]. Although ablative therapy is generally considered only after drugs

have failed due to the fact that catheter ablation is an invasive procedure with attendant potential hazards, including procedural stroke and pulmonary vein stenosis [17]. It is worth-noting that RFA can be useful, but its use may be limited because of complications.

The main question can arise that how safe RF catheter ablation is in the treatment of patients with arrhythmias. Certain risks are associated with RF ablation. They carry the prevailing risks of any cardiac catheterization, like thromboembolic complications, infection, bleeding, heart wall perforation, valvular damage, and radiation damage. Besides, particular risks are associated with the ablation procedure itself [18]. Recently presented data from research involving patients who had earlier not responded to antiarrhythmic drug therapy suggests that patients who underwent catheter-based AF ablation had remarkably less AF during follow-up than those who received more antiarrhythmic drug therapy [19].

Radiofrequency catheter ablation (RFA) has revoulutnlized in the treatment of atrial fibrillation (AF) and is globally accepted and more effective than antiarrhythmic drug (AAD) therapy [20]. It is worth noting that both AAD therapy and RFA procedure can bring along complications and adverse outcomes concerning their safety and it is on the increase [21]. According to the statistics released by seventy-two centers located in 10 European countries on 1391 patients underwent an arterial fibrillation ablation procedure between October 2010 and May 2011, 21% referred to the center due to the post-ablation arrhythmia, and 40% successfully were treated without AAD, 18% of the patients needed a second ablation procedure, following that 2.5 % of the patients faced adverse complications [22].

Considering the current debates on RFA procedure, it is still counted as the first-picked treatment for the patients suffering from atrial fibrillation[23]. Fig. 5 demonstrates the schematic of the radio-frequency ablation (RFA) catheter in the treatment of atrial fibrillation (AF).

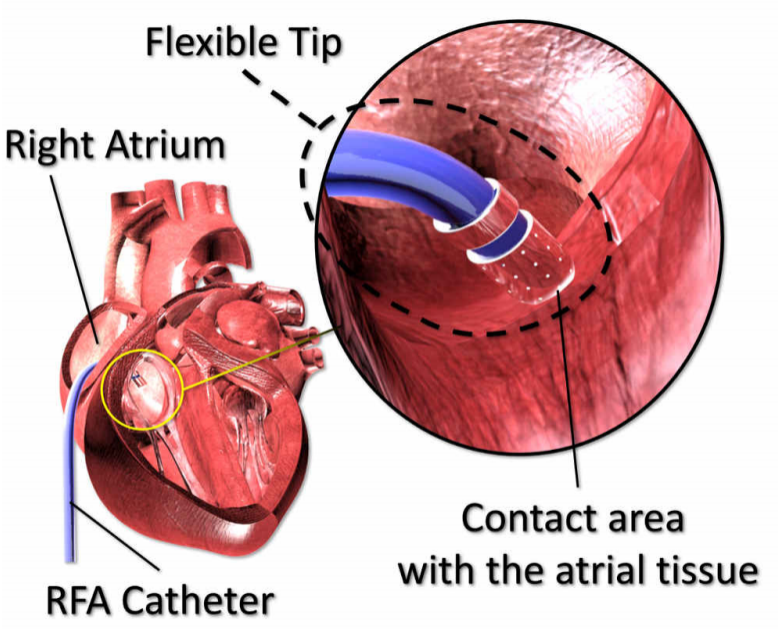

Figure 5: Radio-frequency ablation catheter in contact with the heart tissue that causes abnormal electrical pathways in atrial fibrillation (AF) [24].

1.4 Artificial Intelligence

The primary purpose of this thesis is to tackle the limitations of the sensor-based and model-based approaches in MIS to estimate the contact force at the catheter tip. Artificial Intelligence (AI) was applied in this study and contributed to contact force estimation with high accuracy.

Machine learning (ML) algorithm is a branch of artificial intelligence (Fig. 7). ML is one of the ways we expect to achieve AI. ML constitutes a series of methods in which they can correctly interpret external data and learn the data and use this learning to accomplish particular objectives[25]. In other words, ML relies on dealing with small to large datasets by analyzing and correlating the data to detect general patterns. It was first introduced by Gregory Powell and Mike Donavan and is traced back to the 1940s. Artificial intelligence is broadly categorized into machine learning and deep learning (Fig. 6).

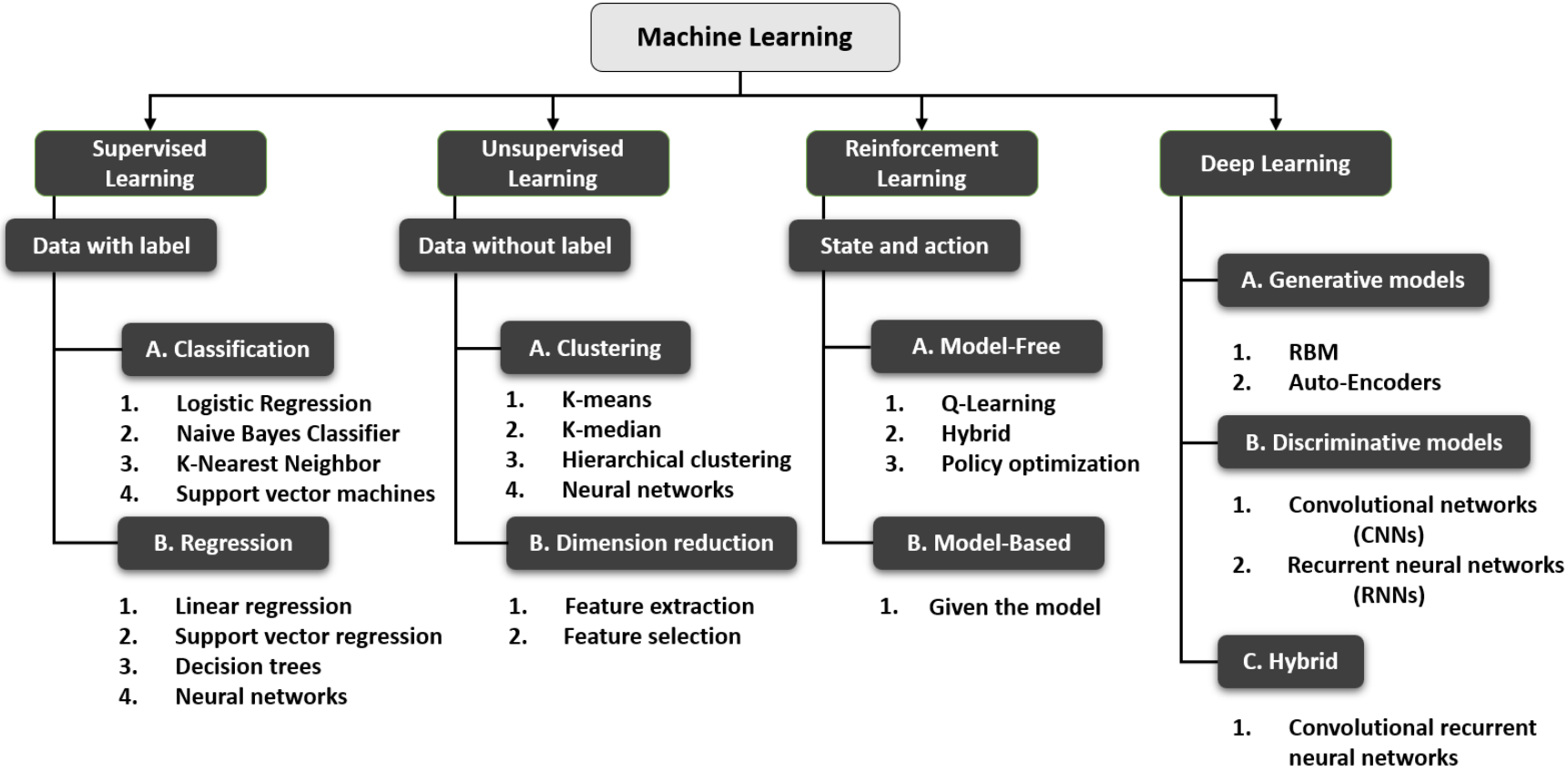

Figure 6: Overview diagram of machine learning algorithms.

1.4.1 Machine Learning Technologies and Techniques

Machine learning is a multipurpose approach of artificial intelligence that can learn relationships from the data without needing to identify them [26]. Machine learning is described by three types of parameters based on the learning rules such as supervised, unsupervised, and reinforcement [27]. Machine learning performs classification tasks clearly and efficiently because of its architectural design and learning methods. There is no unique algorithm since learning algorithms differ in their learning capabilities.

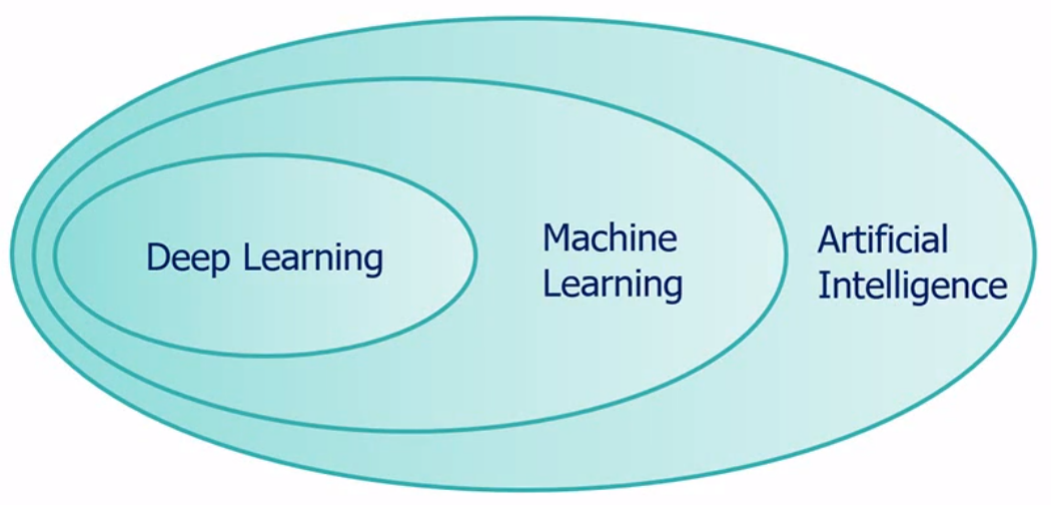

Figure 7: Definition of artificial intelligence

The main appeal will be the capability to derive predictive models without a necessity for strong assumptions about the primary mechanisms that are generally unfamiliar or insufficiently stated[28].

In supervised learning, the system is supplied with large amounts of data through its training state, which directs the system to output what should be achieved from each particular input amount. The trained model is then evaluated with test data to validate the result of the training and measure the accuracy. In general, supervised learning is based on modeling the relationships and dependencies between the target prediction output and the input features. We can predict the output amounts for new data based on those associations, which it has learned from earlier datasets supplied.

Supervised learning methods perform great at regression and classification problems; supervised learning aims to make a connection between the input data to particular measurements. In contrast, unsupervised learning algorithms have no output classes or labels on the data (the model is trained with unlabeled data). Algorithms can operate freely to learn more about the data and present blind output values. Unsupervised learning is prevalent in clustering applications and data representation (the act of predicting rules that describe the data). In other words, the unsupervised learning model recognizes the pattern of the input data. Reinforcement learning learns by trial and error communications with an environment based on the reward/penalty assignment. Reinforcement learning focuses on intelligent agents to deal with an environment, and the feedback received from its actions [27].

Fig. 6 demonstrates various ML methods and techniques, including Decision Trees (DTs)[29], Artificial Neural Networks (ANNs)[30], Support Vector Machines (SVMs)[31], K-nearest Neighbors (KNN)[32], and K-means [33].

1.4.2 Medical Applications

The learning-based techniques have been broadly utilized in medical applications. Abdar et al. proposed a computer-aided diagnostic method using a supervised model to predict liver disease in its early stages with an accuracy of 93.75% [34]. Besides, Abdar et al. introduced a machine learning algorithm, including a Support Vector Machine (SVM), to diagnose Parkinson's disease with an average accuracy of 99.18% [35]. Also, to diagnose Wart, which is known as a skin disease, ML techniques such as linear support vector machine (SVM) and random forest algorithms were applied with an accuracy of (91.11±6.67%) [36].

In another study, a classification of cardiac disorders was proposed using electrocardiography (ECG) signal analysis using support vector machine (SVM) classifier.

This research was done based on ECG signals' fragments from the MIT-BIH arrhythmia database from 29 patients. The model accuracy obtained from this study was 98.99% [37]. E.Bron et al. also introduced a computer-aided SVM (Support Vector Machine) classification model with an accuracy of 90% for Frontotemporal Dementia (FTD), including Cognitive Normal (CN), Mild Cognitive Impairment (MCI) and Alzheimer's Disease (AD), which underlying dementia using neuroimages taken by MRI[38].

Deep learning differs from regular machine learning in just how representations are learned from the raw data. In reality, deep learning enables computational models consisting of many neural network-based processing layers to learn complex and abstract features [39]. The number of hidden layers, their interactions, and the capacity to learn meaningful features of the inputs are the main differences between deep learning and conventional artificial neural networks (ANNs).

Indeed, typical ANNs are normally restricted to three layers and equipped to attain supervised interpretations, which are only tailored for the particular work, and typically can not be generalized [40]. The deep learning technique has contributed to the diagnosis of diseases in the medical industry. This method utilizes the multi-layer non-linear data processing to recognize feature quantities of texts, images, etc. The key benefit of deep learning is that a highly precise model can be learned from massive data without understanding the comprehensive internal structure[41].

Most of the profound architectures applicable to the health care sector are focused on Convolutional Neural Networks (CNNs)[42], Restricted Boltzmann Machines (RBMs) [43], Autoencoders (AEs)[44], and Recurrent Neural Networks (RNNs)[45].

These approaches fall into different medical usages such as classification of Tumors or lesions, Nodules, Fetuses, Neonates, and Cardiac (Fig. 8).

In deep learning, a Convolutional Neural Network (CNN) is a specific type of Deep Neural Network predominantly deployed to analyze visual imagery. A convolution

layer followed by a pooling layer through an activation function constitutes the fundamental components of a basic CNN. Different architectures such as VGG[46], LeNet[47], AlexNet and ResNet[48] have been proposed for CNNs to resolve the emerging issues or improve the performance. The ResNet architecture was employed in the present thesis. The ResNet is one of the most popular architectures for CNNs in which it provides a solution for the vanishing gradient problem. This problem arises in deeper networks with more stacked layers in their architecture. On the one hand, having more layers or deeper networks leads to extract more complex features resulting in a better performance. On the other hand, the vanishing gradient is a barrier to this purpose. Thus, the ResNet stands first among the other architectures to get over this barrier.

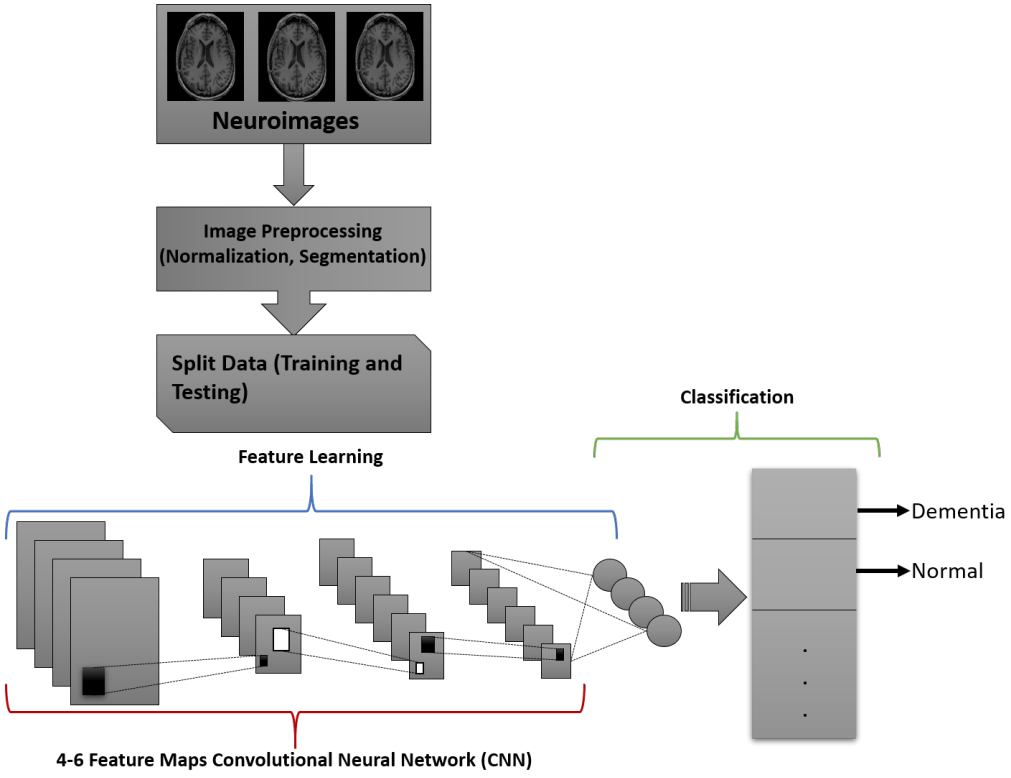

Figure 8: Convolutional Neural Network (CNN) for prognosis dementia classification.

Table 1: The overview of the papers used deep learning approach in medical areas.

Data	**Author**	**Application**	**Model**	**Accuracy**
3D MRI	Prasoon[49]	Automatic segmentation of knee cartilage MRIs to predict the risk of osteoarthritis	CNN	99.93%
Neuroimaging	Liu[50]	Early diagnosis of Alzheimer disease from brain MRIs	AE	88.57%
Retinal images	Gulshan[51]	Detection of diabetic retinopathy in retinal fundus photographs	CNN	99.8%
Images of biopsy	Esteva[52]	Dermatologist-level classification of skin cancer	CNN	93.33%
Ultrasound Imaging	Azizi[53]	Detection of Prostate Cancer	RBM	96.1%
Ultrasound Imaging	Jun Shi[54]	Classification of tumor	AE	96.1%
Shear-wave Elastography	Qi Zhang[55]	Classification of breast tumors	RBM	96.1%
ECG signals	Acharya[56]	Detection of myocardial infarction	RBM	96.1%
Heart sound	Rubin[57]	Recognizing abnormalities in heart sounds	RBM	96.1%
Coronary CT angiography	Zreik [58]	Identification of patients with functionally significant coronary artery stenosis	RBM	71%
Patient note	Dernoncourt[59]	De-identification of patient clinical notes	RNN	96.1%
Photoplethysmogram (PPG)	Jindal[60]	dentification of patients with functionally significant coronary artery stenosis	RBM	96.1%

1.5 Research Objectives

The introduction and review section illustrated the use of machine learning and deep learning underlying artificial intelligence are promising approaches in many medical areas. Utilizing AI could help surgeons to predict catheter-tissue contact force in catheterization in minimally invasive surgery (MIS). This thesis has aimed to estimate the contact force at the catheter tip using machine learning and deep learning approaches. The first chapter has proposed a machine learning catheter-tissue contact force method. A regression model can predict the contact force based on the deflected shapes of the catheter tip section image that yield specific curvature coefficients and corresponding contact force. The second chapter introduces a convolutional neural network (CNN) that extracts the catheter's deflections through images and renders them to the corresponding force. The proposed deep learning model can make the prediction relying on the input images without needing feature extraction and preprocessing.

1.6 Contribution of the Author

The primary outcomes of the present thesis are one journal paper and an IEEE conference paper. The first paper has been submitted to the Journal of American Society of Mechanical Engineers (ASME). The second paper has been submitted to the IEEE International Symposium on Medical Measurements and Applications 2021. The heading and primary technical contributions of these papers are as follows.

1. *American Society of Mechanical Engineers (ASME), Journal of Medical Device*
   Learning-Based Force Estimation for Intracardiac Ablation Catheters
   The main contribution of the work is to develop a learning model to estimate

the catheter-tissue contact force without prior information of mechanical properties of ablation catheters.

2. *IEEE International Symposium on Medical Measurements and Applications*
   A Deep Learning Force Estimator System for Intracardiac Catheters
   The primary contribution of this study is to develop a deep learning model to estimate the catheter-tissue contact force. The model can make predictions based on the input images without utilizing any feature extraction or pre-processing.

1.7 Organization of the Thesis

This thesis is presented in a manuscript-based format. It involves one journal paper in the third chapter and an IEEE conference paper in the fourth chapter. All chapters, excluding the first two and last chapters, have been replicated from the papers mentioned above that are under review. The first chapter addresses the introduction and problem definition and maneuvers over arrhythmia and the second chapter introduces the different approaches to estimate the catheter-tissue contact force. The last chapter presents the conclusive remarks about the contributions and future works.

Chapter 2

Literature Review

2.1 Trends in the Adoption of Robotic Surgery

Robotic-assisted intervention facilitates an accurate range of device positioning and radiation protection for both physicians and patients. This system is used to navigate the catheter through the vessels for vascular applications. This device includes friction wheels to grip and rotate the catheter (Fig. 9). The Corpath robotic-assisted surgery system was developed by Corindus Vascular Robotics™[61]. This robotic platform was designed for surgeons to improve their precision in maneuverability during the catheterization and intervention. Within intervention, the physicians sit behind a workstation and hold a set of joystick controls that translate the physician's actions into device control.

The Sensei and Magellanrobot systems™was designed by Hansen Medical[62]. This system contains a robotic arm at the patient table and a remote physician console, which is away from the radiation source. This system benefits from catheters equipped with a sheath. It also carries advantages such as intravascular shaping, solid stability, center-line driving, and remote navigation, following that precision at distal tip control is significantly accurate (Fig. 10).

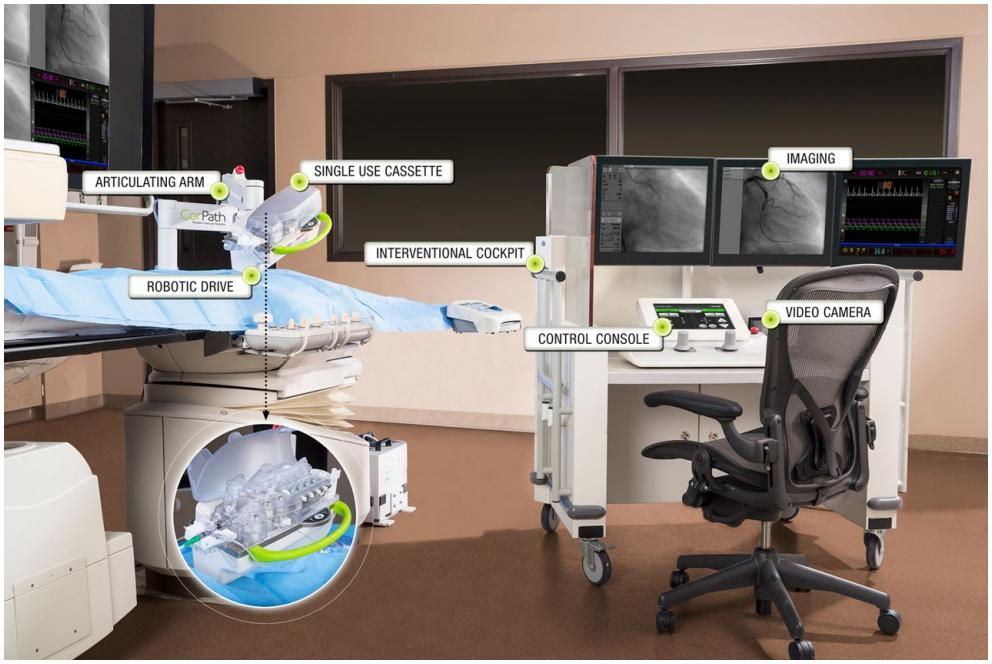

Figure 9: The Corpath remote robotic control console positioned within the interventional cockpit, table side-mounted robotic drive, and single-use cassette (inset) (Courtesy of Siemens Healthineer-Corindus Inc.)

Amigo robot system ™[63] was designed in Catheter robotics Inc. This robotic-assisted surgery is a remote catheter system was equipped with three degrees of freedom (DOF) manipulation arm that a steerable catheter is implemented on the slave side, and wireless control is provided to the interventionist navigation. Amigo is a platform that accommodates all types of commercially steerable catheters in the market (Fig. 11).

The Niobe robot system ™, designed and developed by Stereotaxis Inc [64] a leader in the robotic industry to treat cardiac arrhythmias, has introduced this system provides a reliable and accurate magnetic navigation motion in catheter during the intervention. This system uses the two controlled magnetic arms on the patient's sides to control navigating a catheter linked to the magnet (Fig. 12).

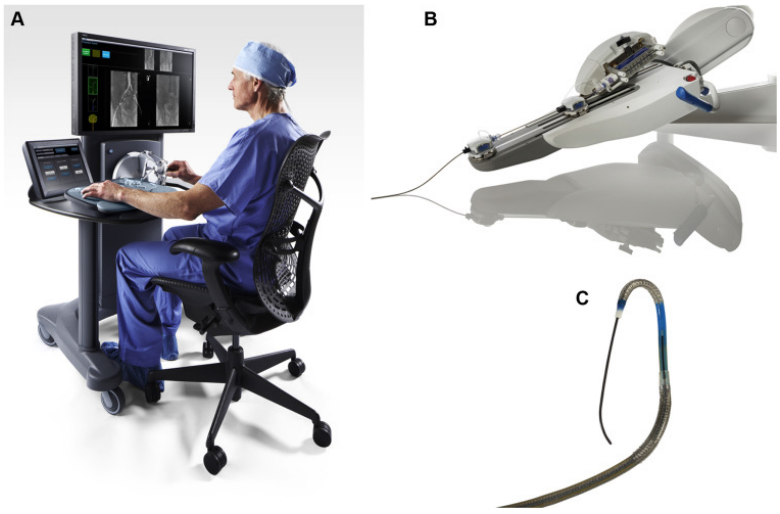

Figure 10: (a) Remote physician console, (b) Sensei and Magellanrobot systems, and (c) catheters equipped with sheath and low profile, for navigation in smaller vessels (Courtesy of Hansen Medical Inc.)

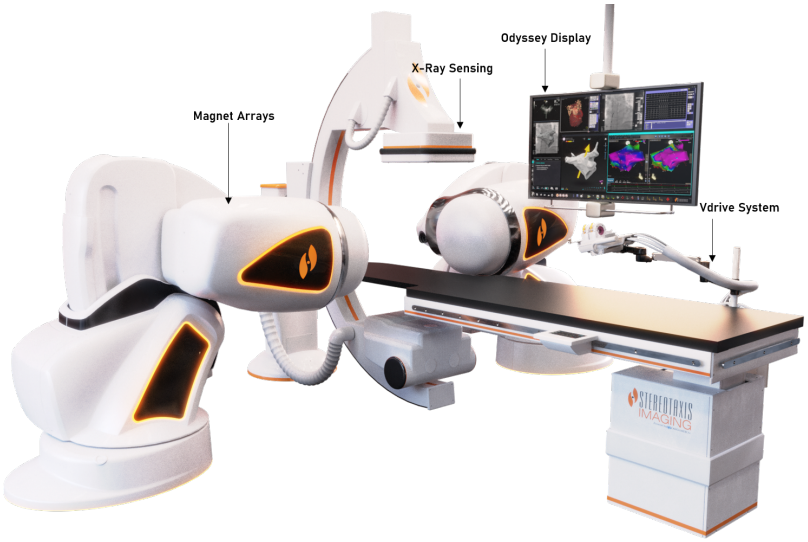

Figure 12: Stereotaxis robotic magnetic navigation system and imaging system (Courtesy of Stereotaxis Inc).

Furthermore, da Vinci Surgical System™is a minimally invasive surgical robot made by the company Intuitive Surgical. This system provides the surgeon with a set of instruments to conduct robotic-assisted minimally invasive surgery. Da Vinci acts as the surgeon's hand motions such as rotating and bending in real-time. the Da Vinci system also renders the high 3D resolution views of the surgical area and

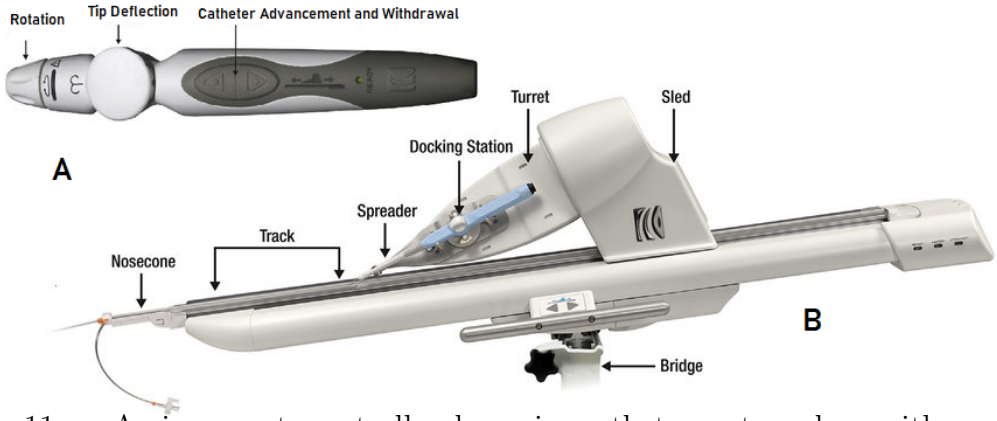

Figure 11: a: Amigo remote controller, b: amigo catheter system along with a catheter implemented into the robotic arm (Courtesy of Catheter Precision Inc.)

incisions (Fig. 13)

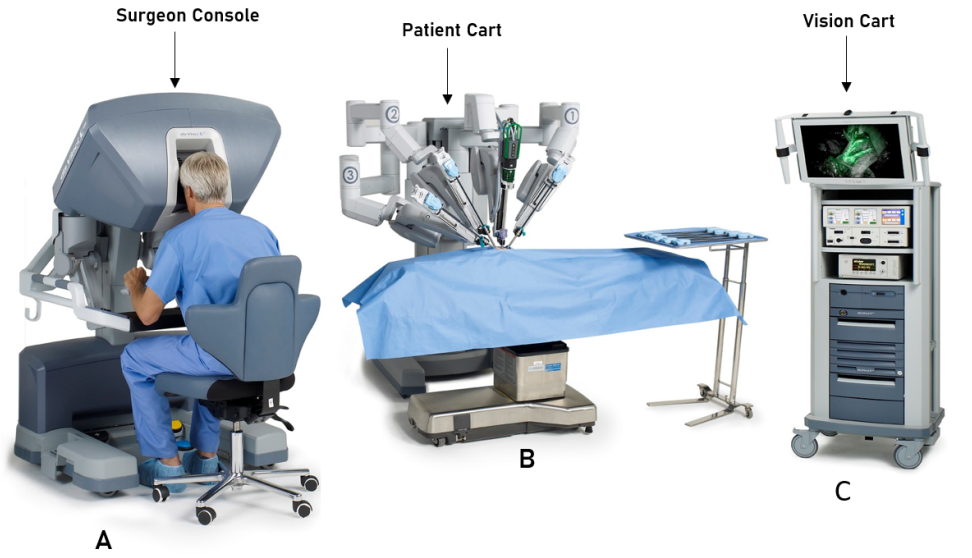

Figure 13: (a) Controlling the instruments while monitoring surgical areas and incisions, (b) patient card positioned beside the patient and includes the instruments and the camera controlled by the surgeon, and (c) 3D vision cart (Courtesy of Da Vinci Intuitive Inc.)

2.2 Necessity of Estimation the Contact Force

Haptic generally represents touch feedback, including kinesthetic (force) and cutaneous (tactile) feedback. Minimally invasive surgery (MIS) and robot-assisted procedures are committed to improving agility while reducing the patients' trauma. Nevertheless, extensive clinical progress with robot-assisted minimally invasive surgery (RMIS) has been marginalized. It is assumed that the contact force feedback has turned into a limiting factor; it is worth noting that all the newly emerged robot-assisted surgical systems while presenting outstanding visual feedback, are ineffective in rendering force feedback. In conventional surgical procedures, surgeons use their tactile and visual capabilities to do open surgery. Still, in robot-assisted minimally invasive surgeries, long instruments are used. They deprive surgeons of the sense of touch, dexterity in insertion, depth perception, tactile cues, and mask force cues [5]. Some studies have been conducted and shown that there is a link between an intra-operative injury and lack of haptic feedback [65]. In robot-assisted minimally invasive surgery (RMIS), all-natural haptic feedback is killed since the surgeon is unable to manipulate the long instruments directly. Lack of force might result in irreparable damages in patients suffering from arrhythmia, and an excessive force can lead to perforating heart tissue, and subsequently insufficient force at catheter tip will cause incomplete treatment [66].

The current force feedback devices for RMIS usually estimate and measure the force applied to patients' tissue by the surgical tools and render the transparent force to the hand through the force feedback mechanism. Commercially available force sensors are efficient in measuring the forces in various telerobotic systems. However, some requirements such as size, geometry, cost, bio-compatibility, and sterilizability must be met because of the restrictions in the surgical environment. The other method is to design the surgical instruments simulating and transferring the force feedback to surgeons' hands. The design of the force sensor can be implemented in the surgical

instruments (Fig. 14) [67] . The conventional force display can be used as force es-

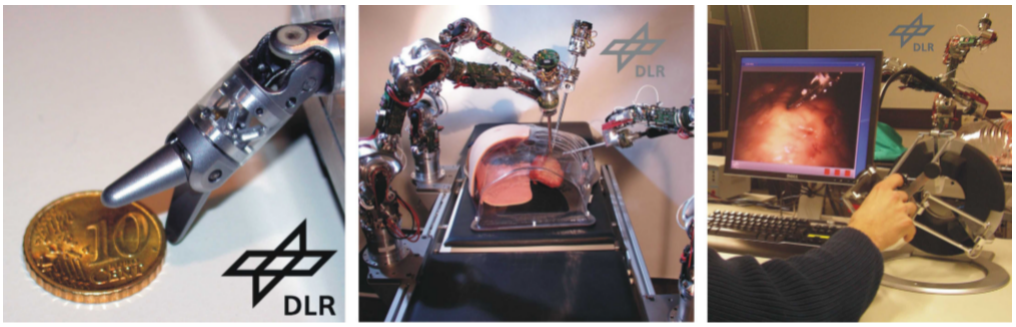

Figure 14: A robotic surgery device for two-hand manipulation with integrated force feedback and 3D vision, designed and developed by researchers at DLR, Germany[67].

timation for surgeons. The master manipulator's actuators are set and programmed to simulate the forces when the robotic arms contact the patients' tissue. Skilled surgical components are typically made as a seven degree-of-freedom (DOF) of motion, such as translational, rotational, and gripping. Nevertheless, the master unit cannot actuate all the degrees of freedom; thus, the system can not render the force feedback in specific directions. The results may be negligible or disturbing, depending on the directions of force feedback missed [68]. The other factor that can affect the accuracy of the force display is the dynamics of the master manipulator; however, a more significant limitation is the trade-off between transparency and stability of the system for force feedback. A perfectly transparent telemanipulator is not possible since it would require perfect models of the dynamics of the patient-side robot and master, zero time delays from computer processing and information transmission.

It is important that small delays and errors in the master manipulator and slave unit can result in uncontrollable misgivings in a "closed-loop" teleoperator. This instability would carry irreparable damages and is not accepted in surgery. An alternative method to measure the contact force is to use sensory substitution. In the most recent years, researchers across the world have developed force-sensing methods and sensor-less force contact estimation methods to test the effectiveness of force and haptic feedback.

2.3 Catheter-tissue Contact Force Estimation Approaches

Cardiovascular diseases (CVDs) stand first among the other conditions to jeopardize people's lives worldwide and the main cause to bring about more mortality. Catheterization procedure, along with accurate haptic feedback, is a primary treatment for CVDs. Traditionally, interventionists would rely on X-ray imaging to measure the contact force indirectly [69]. Haptic feedback in model-based approaches is rooted in the catheter's mechanical model and changes in patients' tissue. Many studies have been carried out to estimate the contact force based on catheters' mechanical characteristics and guidewires. These components are manufactured of coils. They are made of biocompatible materials like Tungsten Nickel-Titanium alloys, Gold, or Platinum [70]. Catheters and guidewires are considered single-dimension materials. It is hypothesized that diverse approaches have been gone through to model the catheters: multibody dynamics, particle-based models, and Continuum mechanics models.

2.3.1 Instrumented Cardiac Catheters (sensor-based)

In recent years, many tactile sensors have been developed to facilitate force measurement in MIS/RMIS procedures. The application and use of the sensors necessitate physical and technical requirements. Consequently, the application and implementation factors must be weighed when selecting a sensing concept. Initially, researchers must define and give priority to the use-case of the sensor before developing the sensor. The structure of MIS and RMIS tactile sensors are electrical-based[8]. These tactile sensors are divided into four categories, such as piezoresistive, piezoelectric, capacitive, and optical sensors (see Table 2).

As mentioned, MIS carries many advantages and is of great importance that has motivated researchers across the world to carry out studies to increase the dexterity in

MIS procedures and priority is given to MIS over conventional surgeries because of less discharging time of the patients and minimal lesion, minimizing trauma particularly for those suffering from anemia. Lack of haptic (force and tactile) feedback provided to surgeons is considered a major limiting factor in MIS. Many other sensor-less and model-based force estimation methods have been done. Sensor-less methods bring along mathematical complications in simulating the catheters and guide-wires and requiring the extraction of catheters' mechanical properties, vessels, solution schema, and motion of the vasculature discretization length. Besides, the use of sensors to estimate the force at the tip of the catheter tip requires miniaturization of the sensor over the cardiovascular catheter. This may carry barriers to building the sensors, such as sizing, MRI (Magnetic Resonance Imaging) compatibility, and the catheter's structural flexibility. In contrast with model-based approaches, sensor-based methods are less dependent on unknown mechanical parameters such as the catheter's stiffness or structure. They can provide fast feedback to surgeons. It is worth noting that the availability of sensor-embedded catheters and high cost are considered the limitations of the sensor-based system.

2.3.2 Model-based Force Estimation Methods (sensor-less)

2.3.2.1 Multi-body Dynamics Models

Shapes of the guidewire inside the human body can be simulated by parameterization-based algorithms, which are efficient and precise [71]. This algorithm is rooted in elementary physics and yields a reasonable accuracy. This model is acceptable and utilized in modeling the deflection and motion of slender structures such as catheters and guidewires [71]. To derive the kinematic equations of the deformable body, the structure is assumed to be a set of rigid bodies connected by spherical joints, including springs and/or dampers. This approach is known as the Multi-body model method

[72]. This approach simulates the minimally invasive vascular interventions and models a discrete design of a guidewire and catheters with different physical features [73]. Another study to estimate the contact force that is computationally considered an efficient algorithm for training purposes is modeling the blood vessels and catheters that enable interventionists to have a haptic sense while manipulating the catheter in the virtual procedures. In this method, the Finite Element Methods (FEM) were used to model the tissue-deformable behavior [74].

2.3.2.2 Particle-Based Dynamics Models

Mass-spring models or particle-based models are applicable for modeling objects with complicated material features like non-linearity and viscoelasticity. They have been chiefly utilized to acquire the deformation of vascular tissue [75]. Many studies have been carried out to model the catheter and guide-wire using this method [76]. A catheter can be modeled using the mass-spring method, the method decomposes the image of the guide-wire and catheter into the model that is defined as a set of beam elements and animation component, and physical interaction between guide-wire and catheter is performed using gap technique, on the other hand, the vessels are assumed as a rigid object, in other words, a novel model to interactively simulate a catheter and a guide-wire. This model presents realistic performances for the two simulated objects and improves the model with a particular visualization method [77]. Notwithstanding the acceptable performance in computational, mass-spring models are not physically reliable.

2.3.2.3 Continuum Mechanics Models

Camarillo et al. [78] revealed a continuum model of a tendon-driven catheter in early developments. A promising achievement in predicting the catheter's deflection shape under quasi-static manipulation was shown. Baily and Amirat showed a continuous

representation of statistic deflection in the intracardiac catheter intervention (MALICA) in 2005. Nevertheless, the models mentioned above were not presented in the real-time platform and considered quasi-static conditions; furthermore, the models needed precise structural data, e.g., non-linear material compliance and measurement of the force catheter tip [79]. The quasi-static condition is far away from the cardiac vessels' physiologic conditions. It presents the above models as ineffectual for robotic PCI (Percutaneous Coronary Intervention) purposes.

Khoshnam et al. [80] introduced the continuum deflection model in 2012, and the large deflection of steerable ablation catheter was modeled using the Bernoulli-Euler beam theory (e.g., see [81] for details).

The shear stress of the cross-section was neglected in the study. This hypothesis appears logical because of the catheters' high slenderness; however, the model was based on a quasi-static theory.

Furthermore, khoshnalm et al.[82] has claimed successful implementation of the large deflection study method proposed in [80] to predict contact forces at the tip of an ablation catheter with the steady-state error of less than 5%. Although their outcomes were encouraging concerning the precision, their model was not satisfactory considering the various point loads and wall contact conditions through robotic PCI. Besides, their model is assumed to be two-dimensional with the planar cantilever beam. In three-dimensional problems, finding a closed-form solution to a large deformation problem requires accurate examination and simplifies hypotheses; hence, the models using closed-form solutions are generally ineffectual.

A linear finite element model and Bernoulli Euler were proposed to estimate the contact force between an intracardiac catheter and a vascular phantom, including vessels by Gao et al. [83]. The outcomes presented that the model miscalculated the contact force in comparison with other different studies. This is due to the neglect of the nonlinearity generated by the large deformation in the beam[84]. It is worth noting that FEA (Finite Element Analysis) can provide high accuracy in modeling the catheters

and guide-wires. Still, it is highly considered an expensive and vulnerable method towards inaccurate results if insufficient constraints of large deformation and contact analysis are applied to it [8].

2.3.2.4 Imaging, Segmentation, and Shape-Sensing

Recognizing the pixels of an image that exposes the catheter's shape is described as catheter segmentation. The purpose of segmentation is to obtain the catheter's shape and estimate its deformation by caparison to its undeformed original shape. Various approaches have been proposed for catheter segmentation and tracking in X-ray images [85] and cinematographic (video) imaging [86].

To analyze the efficiency of various segmentation methods, Dalvand et al. [87] introduced a set of features, i.e., refresh rate (fps), precision (± 1 mm); in the process, there will be no need for more than two cameras, fiducial markers, auto-calibration, and approximation by circular arcs automatic exposure of the catheter's tip, and 3D remodeling capability. In this method, no need for knowledge of the anatomy and parameterizing of the features is suggested.

2.3.2.5 Curve Parameterization and Estimation of Deformation

In this approach, the catheter shape is parametrized analytically in the formulation [88]. Mainly, curve parametrization is known as the interpolation in three dimensions (x,y,z) that are set of catheter points. In this method catheter is described as a normalized real positive and parameter s in which $s = 0$ represents the tail and $s = 1$ represents the tip of curve[89].

2.3.2.6 Force Estimation Based on X-Ray Image Feed and Shape-Sensing

These techniques are suggested to estimate the catheter's undiscovered acting forces depend on its deformation state (inverse problem). To resolve the problem defining, assembling, and setting the adequate constraints of dynamic equations concerning

the motion and catheter's deformation. Researchers have utilized different methods for expressing the mechanics of the catheter deformation. All of the techniques require the fundamental mechanics' principles such as conservation of momentum (dynamic/static force), conservation of mass, conservation of energy (kinetic, potential, strain, total energy, and external work of the unknown forces. All the factors mentioned are considered as a function of its local deformations. Three principal sets of equations outlined above are needed to tackle this inverse problem; nevertheless, these might result in an irrelevant configuration without appropriate constraints [89].

Chapter 3

Learning-Based Force Estimation for Intracardiac Ablation Catheters

3.1 Introduction

Cardiovascular interventions are treatments that require the diagnosis and rehabilitation of abnormal vessels or heart. Rhythm control with anti-arrhythmic drugs (AAD) is a premier way to treat patients with pre-existing heart failure and atrial fibrillation. Catheter ablation is a well-tested therapy for symptomatic atrial fibrillation that is resistant to drug treatment in patients dealing with abnormal cardiac arrhythmia [90]. Radio-frequency catheter ablation (RFA) is a relatively considered more effective and well-tolerated procedure to cure atrial fibrillation than anti-arrhythmic drug (AAD) therapy. Studies of RFA to cure the patients suffering from atrial fibrillation treatment illustrate higher efficacy rates than studies of AAD therapy and a lower rate of complications [91]. Minimally Invasive Surgery has revolutionized the treatment of cardiovascular disease (CVD). The injury's size is considered minor than in conventional surgery since the slash size is minimal, driving to less discomfort and fast discharge of the patients. Minimally invasive catheter ablation procedure carries several advantages, i.e., minimal incisions, quicker recovery time, reduced bleeding,

and are also considered cost-effective [92]. Physicians need to visualize the patient's anatomy during the catheterization and monitor the catheterization procedures using X-ray fluoroscopy. The use of X-ray fluoroscopic imaging is a radiation source that exposes the interventionists and staff to the scattered radiation. It may jeopardize staff's health in the long run [7]. Thus, it motivates the clinicians to use the MRI imaging systems and researchers to find MRI-compatible tools[93]. The advantages of MRI imaging also expedites developing image-guided therapies and image-based solutions.

3.1.1 Necessity of force estimation

Tool-tissue interaction force is of great importance for cauterization, particularly in Radio-Frequency Ablation (RFA). RFA is known as the premier treatment for atrial fibrillation and arrhythmia. Electrical disruption is the main cause of arrhythmia and changes in heart rhythms[94]. Using imaging and other indicators to assess the causes of arrhythmia is known as electrophysiology (EP) study. An EP study is customarily carried out prior to cardiac ablation to determine the most productive method to treat arrhythmia. The catheters are equipped with electrodes at the pointers that can send electrical impulses to the heart and document the heart's electrical activity. Once a particular heart tissue causing the arrhythmia is identified, the physician will place the ablation catheter tip at an abnormal heart tissue location to create a scar/damage in the tissue that possibly triggers arrhythmia (Fig. 15). In some cases, ablation blocks electrical signals traveling via the heart to terminate the arrhythmia and allows signals to move in a common pathway instead. In ablation therapy, surgeons have no control of knowing how much force is applied to the tissue without force feedback data, which could hinder the surgical task. An excessive force might damage the heart wall, and insufficient force might result in incomplete ablation

treatment[66]. The safe limit of force at the tip of ablation catheters is $0.3N$, and over-loading may result in puncture of the heart chamber and damages to the vessels. Besides, catheter tip contact force must retain about $0.1N$ to gain effective treatment for RFA therapy [95].

Robot-assisted cardiovascular devices have also been developed and utilized to increase the dexterity in tip motion and provide excellent visual feedback [96]. However, they are inadequate in presenting force data or feedback. Robot-assisted cardiovascular devices are categorized for three main procedures: Percutaneous Coronary Intervention (PCI), Percutaneous Peripheral Intervention (PPI), Electrophysiologic Intervention (EPI). Different remote-control robotic devices such as CorPath200 ™, CorPathGRX™, Niobe™, and Sensei™ robotics catheter system were introduced and used in the medical industry to eliminate the potential risks during conventional cardiovascular procedures. The applicability of these devices for radio-frequency and electrophysiological mapping ablation was studied in 2003 by Ernst et al.[97]. Some researchers carried out studies concerning the force measurement using direct and indirect approaches such as embedded force sensing elements and model-based methods.

To collect force information during an RFA procedure, sensing elements have been embedded at the tip of ablation catheters, such as piezo-resistive [98], optical[99], capacitive [100] and piezo-electric[101] sensor systems. Optical sensors are MRI compatible and fall into three categories Fabry-Perot Interferometry (FPI), Fiber Bragg Grating (FBG), and Light Intensity Modulation (LIM). FPI and FBG-based sensors are sensitive to temperature and the DAQ (Data Acquisition) device to collect the data is costly. LIM-based sensors provide accurate data, but they are less sensitive [102]. The sensors containing the piezo-resistive, piezo-electric, and capacitive are not MRI compatible because of the metal materials used in these types of sensors[102]. Nearby ferrous materials, e.g., braiding of the sheath and nearby circular mapping

catheters, may affect the force measurement accuracy of sensorized catheters. However, MRI affects ferromagnetic components' functionality and specifically catheters equipped with a force sensor[103]. TactiCath™ and Imricor ™ [104] are the MRI compatible steerable diagnostic/ablation catheters equipped with a optical force sensor. Utilizing these types of catheters in the RFA procedure has shown that real-time contact force technology boosts the ablation effectiveness and treatment of supraventricular tachycardia and atrial fibrillation by allowing better control of lesion size [105]. However, force sensors add more complexity to the structure of the ablation catheters and can reduce the instrument's reliability and deliverability [105]. Moreover, the size limit and sterilizability of sensors mounted in RFA catheters are considered critical problems[106].

Sensor-less methods have been introduced and are categorized into continuum mechanics, differential geometry, and particle-based dynamics.

One of the force estimation approaches is based on shape estimation of the ablation

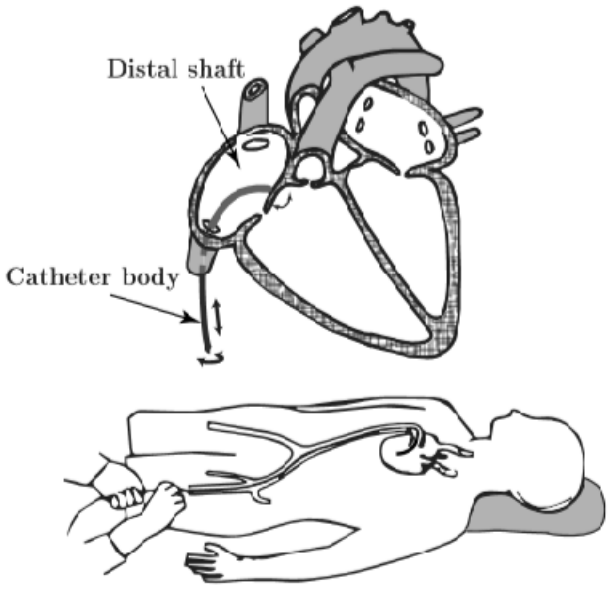

Figure 15: Intracardiac intervention procedure [107].

catheters using two electromagnetic sensors and designing a kinematic redundancy manipulator of the catheter model that could estimate the force at points or multiple points [108]. Predictive modeling for microwave ablation procedure has been developed to estimate the contact force as well [109].

Another study proposed obtaining the catheter model's known parameters based on pose measurement of the distal tip to estimate contact force [107]. A nonlinear material model of heart tissue has been proposed in which, based on the tip displacement and tendon lengths, the force at catheter's tip on the heart tissue can be measured [110].

Other studies suggest that the information on the contact force can be collected from the changes in the catheter's shape/position and orientation of the distal shaft, where the contact force can be controlled by altering the flexion of the distal shaft [111]. Multi-point contact force estimation at the tip and side of the catheter has been proposed using image-based numerical methods [112], where a finite-element model of a catheter is fed by image data to simulate the navigation procedure and estimate the forces. Also, a kinematic multi-section model of the tendon-driven for catheter deflection in 3D was developed to estimate the contact force by the shape estimation with tracking of the catheter tip position and tension feedback [113].

Table 2 compares studies cornering instrumented and model-less force-sensing methods, their application, advantages, and limitations. The sensor-based approaches have fewer ambiguous model parameters but necessitate changes in prevailing tendon-driven catheters' configuration and layout. On the other hand, the sensor-less approaches are less tedious to incorporate, but they need a precise simulation of the catheter dynamics and typically include model parameters with uncertainty.

This work proposes a novel sensor-less force estimation technique based on the machine learning algorithm, which uses the image of the catheter distal tip section. Learning methods have also been used in needle insertion to estimate the force at the needle tip [114] and other robotic-assisted tools [115].

The proposed approach utilizes learning the shape of the distal catheter section by extracting the deflected shape features and estimating the force that corresponds to those features. Employed shape features were determined as the polynomial coefficient of a curve fitted to catheter distal shape as being deflected in contact with heart tissue. The surgeon controls the force during the ablation procedure based on the estimated force obtained from the learning model.

The paper begins with developing a methodology to generate an estimation model for tip contact force based on imaging data. The learning model employs a non-linear support vector regression algorithm, which uses catheter knob and shape features data as inputs and forces data as the target. An experimental setup is designed to simulate a catheter tip in contact with artificial heart tissue. The setup has a two-degree-of-freedom heart motion simulator to mimic heartbeat movements, which simulate changes in contact force based on inducing deflection to the catheter distal tip section. Artificial heart tissue mounted on a six-axis force/torque sensor to record tip-tissue contact forces.

The prepared model was trained using a set of collected data. For validation purposes, the trained model estimated contact forces based on shape features and catheter knob in an unseen testing data set. Then estimations are compared to their observed force values. The model generated in this study is for a specific ablation catheter and artificial tissue for proof-of-concept. To carry out, the following steps are needed: data collection (force, images of distal section and catheter knob angle), image processing and feature extraction, developing and training the model, and model evaluation in estimation.

This method can be an alternative force-sensing solution since the difficulties associated with sensor integration is avoided. The proposed technique is computationally efficient and convergent for real-time applications without complexity and dependency to the catheter mechanic models. To the best of our knowledge, this is the first study that uses the learning method to estimate the contact force at the ablation catheter's

tip.

Table 2: Comparison of the sensor-based and model-based force estimation methods.

Approach	Method	Author	Application	Advantages	Limitations
Sensor-based	C	Kim[100] Golpayegani[116]	RMIS	Accuracy = 98.1 % Sensitivity = 0.83 kHz/N	Not MRI Compatible Electrical passive
	PE	Qasaimeh[117] Ju[118]	Catheterization Catheterization	Force Range = 0.01- 4N Error < 3.5%	
	PR	Hwang[119] Kalantari[120]	RMIS Catheteirzaion	Linearity > 99.6% RMSE = 0.611 N	
	OPT	Polygerinos[121] (LIM)	Cardiac ablation	Accuracy = 94% Linearity = 96% Hysteresis = 6%	Low sensitivity
		Yokoyama [122] (FBG)	Cardiac ablation	Resolution = 0.01 N Accuracy = 98%	Temperature sensitive Costly DAQ
		Tohyama [123] (FPI)	Balloon catheters	Force Range = 0 - 0.2 N	
Model-based	CM	Khoshnam[80]	Cardiac ablation	Real-time Imaging	No haptic device Low workspace accessibility
		Khoshnam[82]			Weak energy formulation No haptic device
	DG	Back[124]		Exact energy formulation Real-time Imaging	No haptic device
		Cai[125]		Contact treatment: Augmented Lagrange	Weak energy formulation No haptic device
	P	Lenoir[77]		Contact treatment : Lagrange multipliers	Weak energy formulation, Low workspace accessibility
	MD	Guo[126] Wang[127]		Exact energy formulation, haptic device Exact energy formulation, haptic device	Low workspace accessibility

C: Capacitive, PE: Piezo-electric, PR: Piezo-resistive, OPT: Optical, FBG: Fiber Bragg Grating, LIM: Light Intensity Modulation FPI:Fabry-Perot nterferometry
CM: Continuum Model, P: Particle-based, MD: Multi-body Dynamics, DG: Differential Geometry
PCI: Percutaneous Coronary Intervention

3.2 Methods

3.2.1 Learning-based force estimation

In ablation therapy, cardiologists predict and control catheter-heart tissue contact forces visually by tracking tip deflection under 2D or 3D imaging. It is a learning process based on experiments and training. Here, we are utilizing the same concept to build an image-based learning approach for force estimation. Fig. 16 presents proposed methodology. The overall concept is to train a machine learning model using a set of deflected catheter tip images and their associated contact forces. Any individual measurable property of the catheter-deflected shape varies depending on the tip

contact force, a useful feature. We fit a polynomial curve to the deflected-catheter shape and utilize the polynomial coefficients as quantitative features. Initially, a series of pictures are taken from the catheter tip, i.e., the section which is more likely to be deflected when contacting the heart tissue. A real-time image segmentation extracts deflected catheter shape, followed by curve fitting, which computes the polynomial coefficients of the fitted curve. These coefficients, along with catheter knob actuation angle, are considered as the features for machine learning. The training step is to generate a learning model from the data set of features and the forces. The estimation step is where the model estimates unseen forces from the catheter image and the known knob actuation.

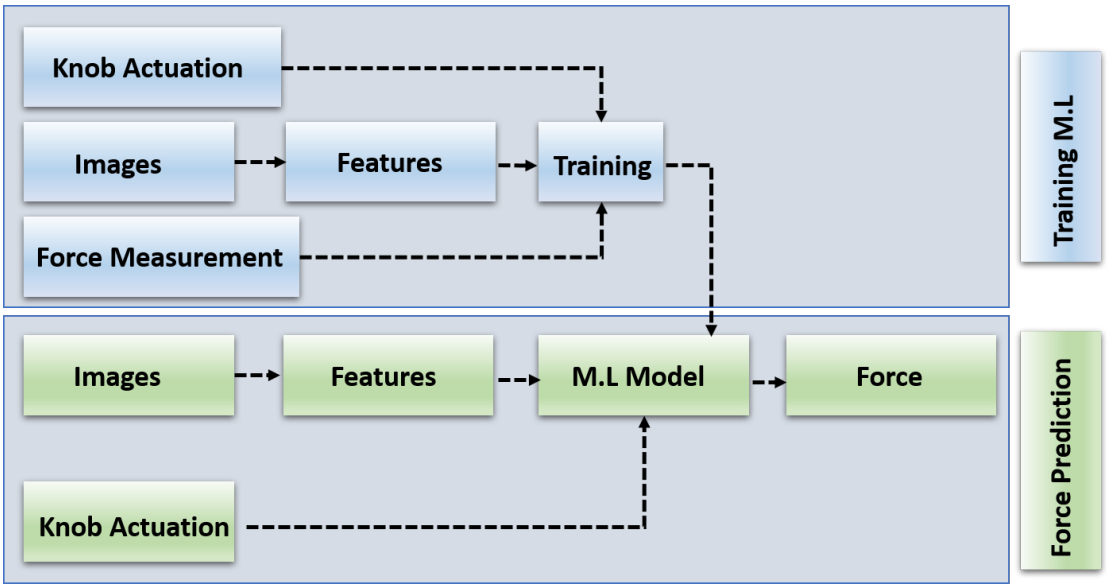

Figure 16: Image-based force estimation through a learning model created by deflected catheter tip shape and knob actuation data.

3.2.2 Image-based shape extraction

The interventionalist provides the initial and final destination in a graphical user interface (GUI) and maintains supervisory control over the insertion, navigation, and tip contact force based on the images obtained. Our method proposes using the

same imaging available in a catheter for force estimation. It is required to extract the pose of the catheter in real-time. To do so, an image processing algorithm has been proposed to segment the catheter's distal end body and track its shape as being deflected by heart tissue. Algorithm 1 explains the proposed image-processing steps. As the global coordinate of catheter image may change case by case in clinical imaging, we are looking at the catheter deflections from the catheter base prospective, isolating it from dependency to the imaging coordinate.

Therefore, a local coordinate is located to the base of the catheter bending section, and pixels are transferred accordingly. An RGB camera collects the image of the catheter in our test setup. The RGB image is converted into a grayscale image (Fig. 17(a)). Thresholding is applied to the grayscale image to create a binary image of the catheter (Fig. 17 (b)). It assigns a black pixel value to each pixel where the density is less than the threshold constant, $Thr = c$. Thresholding helps in effective localizing catheter pixels in the search step (Fig. 17(c)). To form the local catheter coordinate, it is required to find catheter base points. A search step looks for catheter pixels through the initial columns of the frame and fits a line to those pixels. The fitted line to base points creates the X-axis of the local coordinate of the catheter, i.e., the tangent line, and the Y-axis is constructed perpendicular to the existing X-axis. Subsequently, the translation followed by the rotation creates the transformation matrix from frame coordinates to the local catheter coordinates (Fig. 18), which is applied to each point.

$$\begin{bmatrix} x' \\ y' \\ 1 \end{bmatrix} = \begin{bmatrix} R_{2\times2} & T_{2\times1} \\ 0 & 1 \end{bmatrix} \begin{bmatrix} x \\ y \\ 1 \end{bmatrix} \tag{1}$$

where, (x', y') is the local catheter coordinate system, $R_{2\times2}$ is rotation matrix, $T_{2\times1}$ is the translation matrix and (x, y) is the global frame coordinate system. The density of the black pixels of the images has been reduced to optimize the image processing

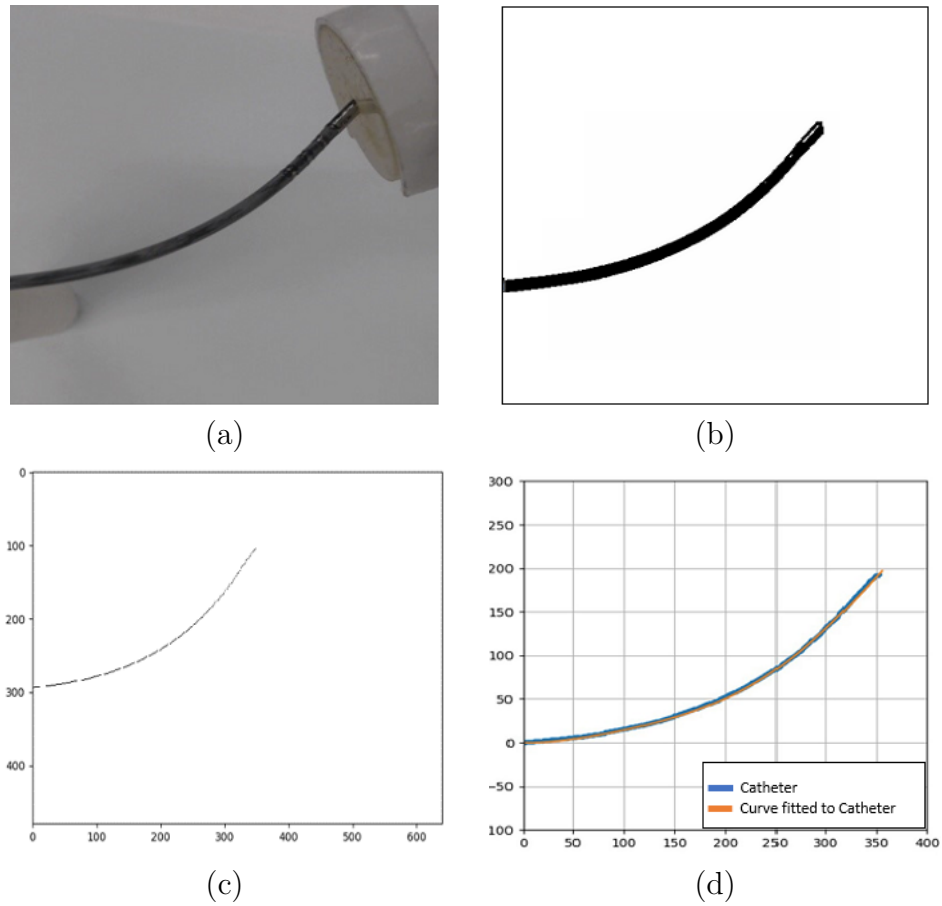

Figure 17: (a) Real catheter image, (b) Binary catheter image, (c) Location of pixels and, (d) Curve fitted to catheter's pixels.

speed, such that the catheter has been mapped to a single-pixel line. Fig. 17 depicts steps of image processing as (a) depicting original catheter image, (b) binary image of the catheter after threshold, (c) catheter single-pixel line, and (d) catheter transformed to the local coordinate.

3.2.3 Curve fitting

The following step is curve fitting, referring to the process of constructing a curve, or a mathematical function, which is best suited to a series of data points. Curve fitting may involve either interpolation where an accurate fitting to the data is required or

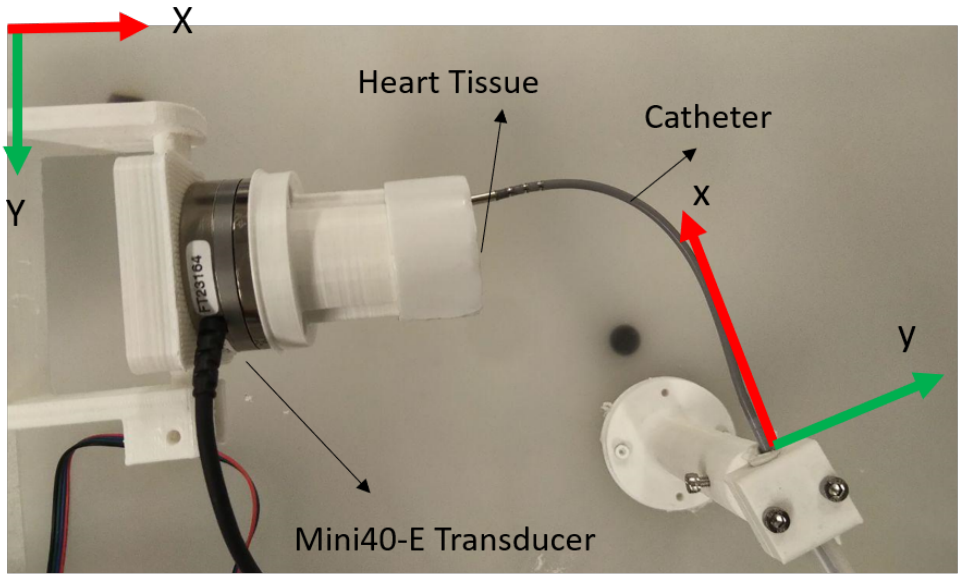

Figure 18: Converting global frame coordinate to local catheter coordinate.

smoothing where a "smooth" function is constructed to fit the data approximately. A fourth-degree polynomial was fitted to extract catheter body pixels to mimic its deflected shape in a mathematical format (Fig. 17(c)). Polynomial gives five unique coefficients corresponding to each catheter shape (C(x)) as Eq. (2). The polynomial coefficient is going to be used as the feature of the catheter image in ML algorithm.

$$C(x) = A_1x^4 + A_2x^3 + A_3x^2 + A_4x + A_5 \tag{2}$$

Fig. 17 (d) shows an example of fitted curve to a deflected catheter.

3.2.4 Learning algorithm using SVRMs

The bent shape of steerable catheters is a function of knob actuation and tip contact force. In this study, we are proposing to estimate tip contact force by tracking the image of catheter distal shape and values of knob actuation. Initially, a learning

Algorithm 1 Image-processing and curve fitting algorithm

Function *Segmentation and Curve Fitting*:
Input: Image of ablation catheter in contact with heart tissue
Output: Coefficients of curve fitted to catheter distal section
Initialization:

$Thr = c$
$BS = N$
while $Frame \leftarrow video.read$ **do** ▷ Image stream LOOP
    $Frame \leftarrow RGB2GRAY(Frame)$ ▷ Color conversion: RGB to grayscale
    $Catheter \leftarrow threshold(Frame, Thr = c)$ ▷ Extracting catheter body pixels through thresholding
    for *columns* 0 to N in catheter binary image scan pixels **do** ▷ Find catheter base point
        if *pixel* ($[P_x, P_y]$) is *black (value=0)* **then**
            Array of BS append $[P_x, P_y]$
    fit line L to BS ▷ Fit a line to catheter base point
    compute the center of points in BS as catheter base reference O ▷ Reference for local coordinate of catheter
    form local coordinate of catheter using O and L
    create $[R, T]$ the transformation matrix to local coordinate of catheter from original *Frame* coordinate
    map $Catheter$ binary image to single-pixel line ▷ This is to optimize the computation cost
    Transfer $Catheter$ pixel matrix to local coordinate of catheter (x', y') using $[R, T]$
    fit a fourth-degree polynomial to $Catheter$ pixel matrix
    return polynomial coefficient of $[c_1, c_2, c_3, c_4, c_5]$

model is prepared to utilize a database of image features (polynomial coefficients) and knob actuation related to corresponding tip contact forces. The SVM algorithm, first introduced by Vladimir Vapnik [128]. Radial Basis function (RBF) kernel function with SVM was chosen in this study considering that the collected data was roughly non-linear. The primary function of SVM is to construct the optimal hyperplane (OH) in the training phase using the proper estimation [129] of a weight vector w and the scalar bias factor b. All of the training models are assumed to be linearly

separable if there exist ω and b such that the following inequalities observed:

$$(\omega \cdot x_i) + b \geq 1; \quad if \quad y_i = 1 \tag{3}$$

$$(\omega \cdot x_i) + b \leq -1; \quad if \quad y_i = -1 \tag{4}$$

where w is weight vector, b is a bias and $\{x_i = x_1, x_2, x_3, ..., x_n\}$ are vectors representing the data points, and y_i are the classes attributes. Feeding this input to the model would enable estimation of force values as system outputs; this stage is called estimation. The estimation model in SVM can be shown as follows:

$$\hat{f}(x) = sign(\omega \cdot \varphi(x) + b) = sign(\sum_{i=1}^{N} \alpha_i y_i . \varphi(x_i) . \varphi(x_j) + b) \tag{5}$$

where, α is the optimization parameter, and product of $\phi(x_i).\phi(x_j)$ is scalar quantity. In machine learning literature, this product is called Kernel Function. SVM can also be used as a regression method, having all the main features that characterize the algorithm (maximal margin). The Support Vector Regression (SVR) applies the same origins as the SVM for classification, with only a few minor variations. The main difference rests with the value of the variable y. For classification problems, the variable y has only two values -1 and 1, that is, $y \in \{+1, -1\}$. However, for regression questions, the variable y can be any real value, that is $y \in R$.

The primary origin of the regression of SVM is to mapping data x to high dimension feature space F by non-linearly mapped φ and have the data linearly regressed in high feature space. Nevertheless, the primary purpose is always the same: to minimize error and individualize the hyperplane, which maximizes the margin; in this method, part of the error is tolerated. Having a generated model, the trained model can be used for estimation purposes. In this paper, the model estimates the force at the tip of the catheter, where input is image specifications and knob actuation angle.

We employed the five polynomial coefficients, the image features, besides the catheter knob actuation as the model inputs. In SVR, $\{.x_i, y_i\}_{i=1}^{N}$ is training data set, in which $x_i \in R^p$ represents p-dimensional input vector following that $y_i \in R$ is a scalar force measured as output. The goal is to develop a function $y = f(x)$ that demonstrates the output force y_i according to the input x_i. The data x is mapped to a higher dimensional feature space F by $\varphi(x)$. The form of this function is:

$$y = w^{T} \varphi(x) + b, \qquad \varphi(x).R^n \to F, \;\; \omega \in F \tag{6}$$

The Support Vector Regression method has been widely depicted in literature [130]. Consequently, only a primary comprehensive summary of the theory underlying SVR modeling will be presented here. The optimization problem and the equality constraints are obtained by the following equations:

$$R_{emp} = C \sum_{i=1}^{N} e(f(x_i) - y_i) \tag{7}$$

subject to :

$$e(x, y, f) = |y - f(x)|_{\epsilon} = \begin{cases} 0 & |f(x) - y| \leq \epsilon \\ |f(x) - y| - \epsilon & |f(x) - y| > \epsilon \end{cases} \tag{8}$$

where $e(x, y, f)$ denotes ϵ-Insensitive Loss Function, R_{emp} is Empirical Risk that needs to be minimized, and constant C illustrates the parameter in optimizing the trad-off between the flatness of the training errors and the model's degree of complexity. The goal is to look for the optimal parameters such as w and b that minimize the estimation error of the regression model. The optimal model will be chosen by having the minimal loss function. The formulation related to the regression in features space might be multi-dimensional, or even infinitive and the problem might not have an easy solution, thus to resolve the issue a capacity control term can be added to the

Empirical Risk Function and yields a Regularized Risk Function as follows :

$$R_{reg} = R_{emp} + \frac{1}{2}\|\omega\|^2 = \sum_{i}^{N} e(f(x_i) - y_i) + \frac{1}{2}\|\omega\|^2 \tag{9}$$

To optimize parameters (w, b), in $R(\omega)$ is Risk Empirical function, the partial differentiation is applied to Eq. (9) with respect to w, b and equate the equations to the zero following that the dual problem can be solved under constrains as follows:

$$\sum_{i}^{N}(\alpha_i - \alpha_i^*) = 0, \qquad 0 \leq \alpha_i, \quad \alpha_i^* \leq C \tag{10}$$

where $i = 1, 2, ..., N$ and α_i, α_i^* are the Lagrangian multipliers, in this stage we attempt to minimize the Eq. (9) for the parameters of α_i and α_i^* under constrains (10) and applying the Lagrangian optimization gives us:

$$\begin{aligned} min(Q_{\alpha_i,\alpha_i^*}) = \frac{1}{2}\sum_{i,j=1}^{N}(\alpha_i^* - \alpha_i)(\alpha_j^* - \alpha_j)K(x_i, x_j) \\ +\epsilon\sum_{i=1}^{N}(\alpha_i^* + \alpha_i) - \sum_{i=1}^{N} y_i(\alpha_i^* - \alpha_i) \end{aligned} \tag{11}$$

and we obtain the optimized values for:

$$\overline{\alpha} = (\overline{\alpha_1}, \overline{\alpha_1^*}, ..., \overline{\alpha_N}, \overline{\alpha_N^*})^T \tag{12}$$

and finally the regression model is generated as fallows:

$$f(x) = \sum_{i=1}^{N}(\overline{\alpha}_i^* - \overline{\alpha}_i)K(x_i, x) + \overline{b} \tag{13}$$

following that $\overline{b}$ is computed in accordance with applying the so called Karush–Kuhn–Tucker (KKT).

$$\overline{b} = y_i - \sum_{i=1}^{N} (\overline{\alpha}_i^* - \overline{\alpha}_i) K(x_i.x_k) + \epsilon \tag{14}$$

where $K(x, x_i)$ is a kernel function , as it was mentioned before we used RBF in this paper. The RBF kernel is defined as follows:

$$K(x, x_i) = exp(-\frac{1}{\sigma^2}\|x - x_i\|^2) \tag{15}$$

where σ is the kernel parameter of RBF kernel.

3.2.5 Experimental setup

Test setup in this study simulates the ablation arrhythmia therapy where the catheter is inserted in vein, in the groin, and navigated to the heart chamber. A heart simulator was designed to replicate heartbeats, and the operator controls the distal section of the tip aimed to reach artificial tissue, e.i., the damaged region of the patient's heart. Experimental setup for data collection and performance evaluation is shown in (Fig. 19). The setup contains a heart motion simulator, catheter contact force measurement platform, camera, Boston Scientific Blazer II XP Temperature ablation catheter, holders/fixtures, and artificial heart tissue. Artificial heart tissue is made of a mixture of silicon rubber that is poured into the designed mold. We aimed to minimize trapped air by degassing the mixture inside the mold using a vacuum chamber. Finally, the mixture was cured at room temperature for 24 hours. The catheter is equipped with the electrodes at the tip to ablate heart tissue and cure arrhythmia. As presented in Fig. 20, the heart motion simulator has two linear actuators equipped with stepper motors (17HS4401-S 40mm Nema) driven by HANPOSE TB660. These two linear actuators are assembled perpendicularly to simulate the 2-DOF motion

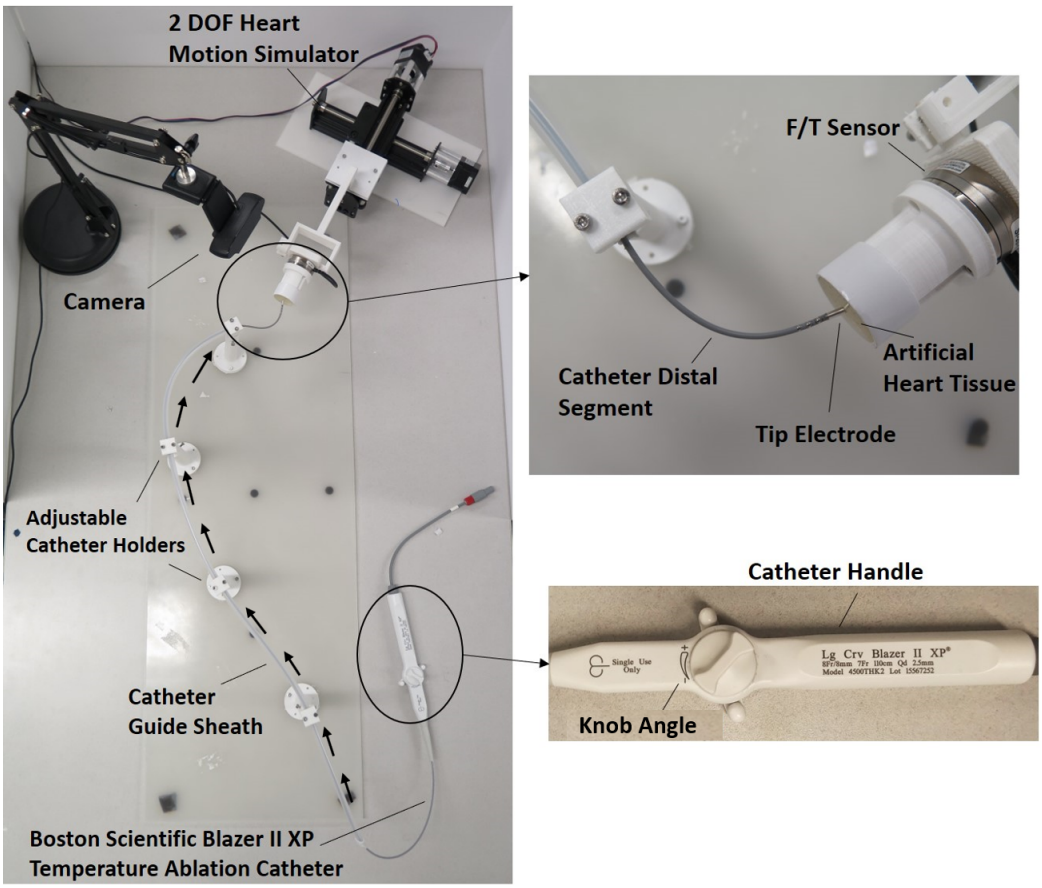

Figure 19: Experimental test setup simulates catheter tip in contact with heart tissue during ablation therapy.

of the heart. Heart motion is briefed as PQRST. P wave indicates atrial depolarization that the atria contract (atrial systole). The QRS complex represents the mixture of S waves, R, and the Q, and also shows ventricular depolarization as well as a contraction (ventricular systole). The PQRST represents a sinusoidal motion of the heart, the designed heart simulator simulates a sinusoidal motion in two directions X and Y (see Fig. 20(b)). A six-axis force/torque sensor (ATI mini 40-E transducer) has been mounted on the heart simulator to record the force while the catheter contacts an artificial tissue. The artificial heart tissue is placed on the F/T sensor to mimic soft catheter-tissue interaction. Catheter path from femoral access, where the interventionalists start inserting, to the heart through the vein is depicted

in Fig. 21. Initially, when ablation catheter enters the left femoral vein and guided to the right atrium (RA) through the inferior vena cava (IVC), it reaches the left atrium via fossa ovalis (FO) and then ablates near the pulmonary veins (PV) (see Fig. 21(b)). The heart simulator represents a 2-DOF motion. Besides, to obtain different deflections at catheter tip in contact with the artificial heart tissue, a similar motion to the half-wave of the PQRST was replicated for the experiments. A similar path is constructed by a sheath and adjustable holders in our setup, which catheter goes through it (see Fig. 19), end of the bending section is fixed as the catheter navigates and goes through the heart wall and this positioning was simulated in the experiments (see Fig. 21(b)). The catheter knob is set at the degree of 10 to induce a pre-deflection in the distal section. It simulates a similar condition to a clinical case where the tip is being deflected to reach in contact with tissue. Then, the heart simulator is run in a sinusoidal forward-lateral motion while the catheter tip stays in contact with artificial tissue. Deflection of catheter changes, and simultaneously, the camera captures the images of the deflected tip section, and the F/T senor records the associated CF. Captured images will be processed to extract the coefficient of the curve fitting as the deflection features. Data of coefficients, knob actuation, and the measured force are prepared for training the model, estimations, and performance evaluation.

3.3 Results

3.3.1 System performance and study protocol

Fig. 22 presents the study protocol from data collection to model evaluation. The collected data from experiments are representing more than hundreds state of deflected catheter which includes five polynomial coefficients, catheter knob angle and

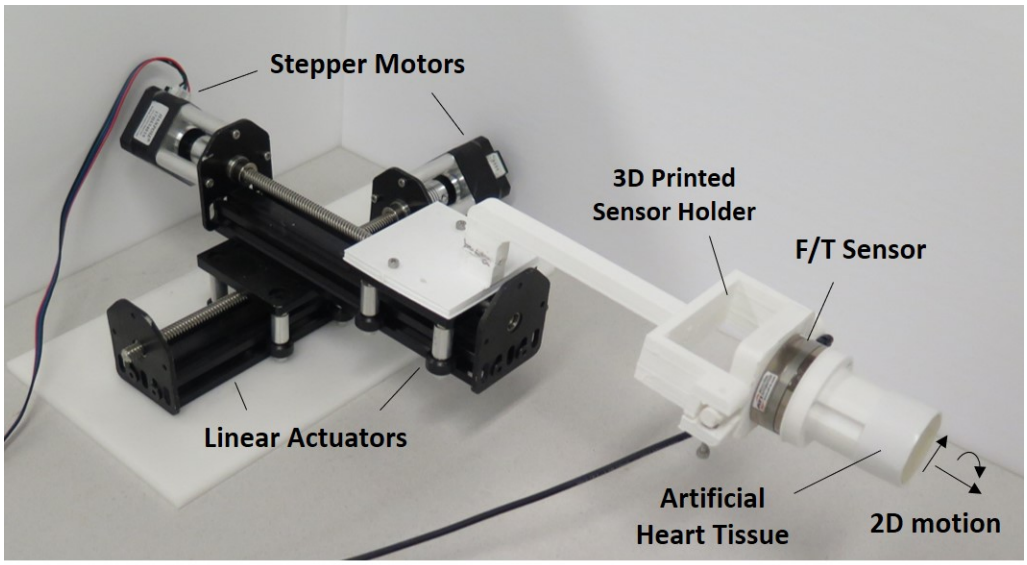

(a)

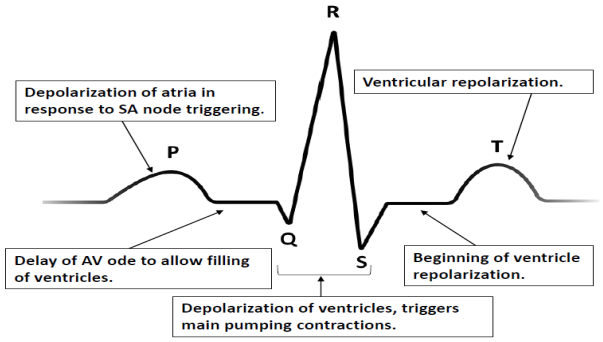

(b)

Figure 20: (a) 2 DOF heart simulator equipped with F/T transducer and artificial tissue, (b) PQRST waveform of a heart in two directions.

associated force. The polynomial coefficients and knob angle are considered as features and the forces represent the target. Data set is separated into training sets and testing sets. From two hundred and twenty data acquired, seventy-five percent of the data are randomly allocated to the training set. Estimations are carried out with twenty-five percent of data left as the testing set. The data is normalized with respect max value for each feature, i.e., coefficients and actuation knob angle. Measured force values are also normalized to the max value. Supervised learning was applied as the

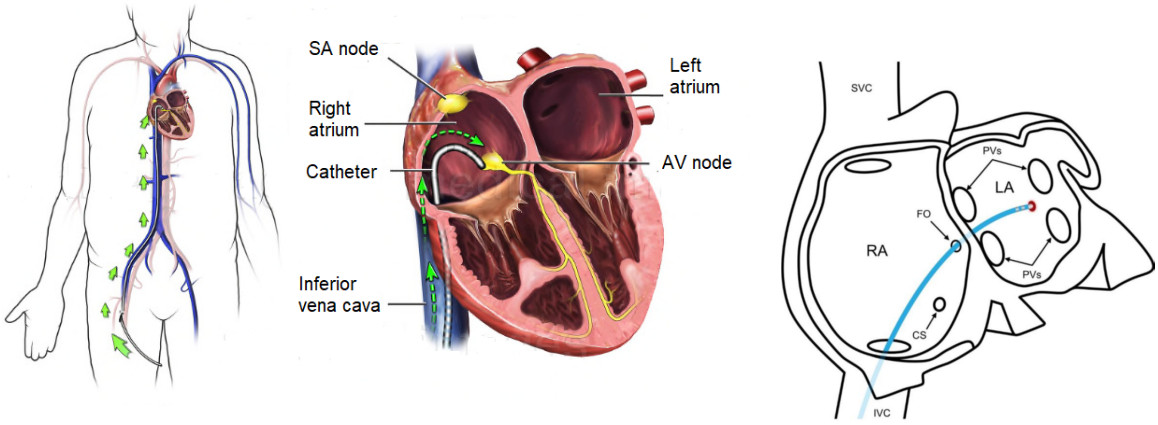

(a) (b)

Figure 21: (a) Sample of cardiac ablation catheter insertion path from femoral access, (b) detailed pathway for ablation [24].

task of learning a function that maps the polynomial coefficients into the measured forces. It brings a common scale, without distorting differences in the ranges of values and it helps to have the same range of values for each of the inputs/outputs of the model. This also guarantees stable convergence of weight and biases. A non-linear SVR model is generated by performing training stage. The regression model is validated then using the testing data set and accuracy of force estimations are evaluated compared to true values. The performance metrics to evaluate our model are including mean-square-error and absolute error of regression loss in estimation step with unseen data.

3.3.2 Experimental learning-based force estimation evaluation

Table 3 shows five samples of normalized data: the coefficients of catheter curve, knob angle and contact force. Carrying out the training stage using the normalized features and labels, the mathematical SVR model is generated.

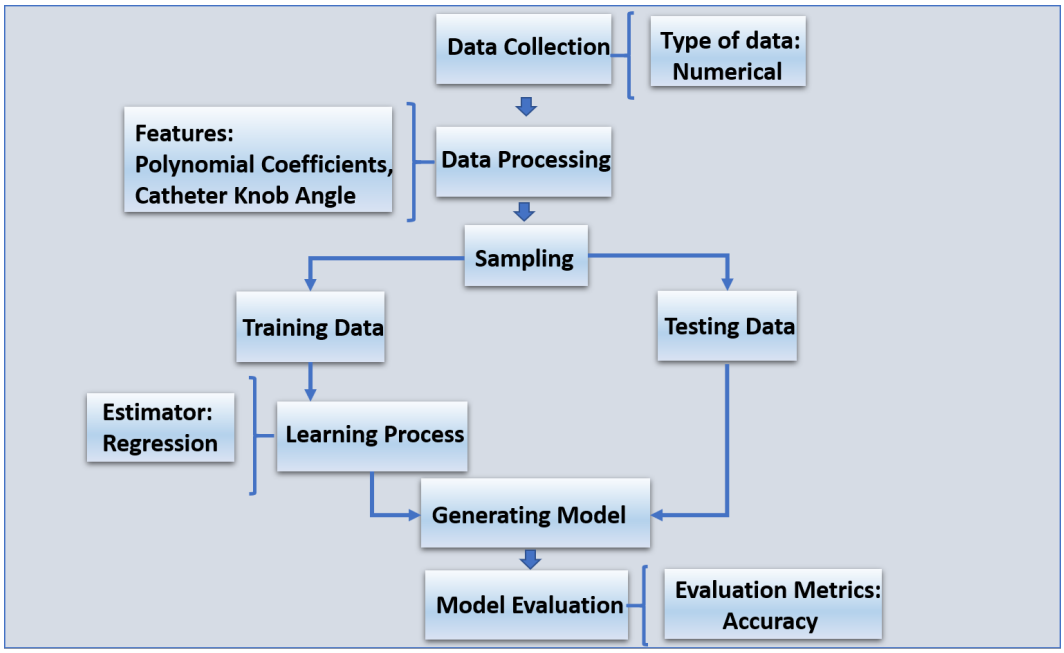

Figure 22: Machine learning flow chart.

Fig. 24 shows fitted SVR model to experimental observed states and force values in training data set. Comparing observed forces to the model suggests that non-linear regression effectively fits the experimental data and mimics catheter tip behavior in contact with heart tissue. Therefore, the model can relate contact force values to the state of the catheter tip section, i.e., coefficient of deflected curve and knob actuation angle. The test data set inputs, i.e., coefficient and knob angle, are fed to the model to predict the contact force of unseen states in order to validate the model. The

Table 3: Samples of normalized data set including five coefficients of fitted curve to the catheter's tip section, knob actuation angle and associated tip contact force.

A_0	A_1	A_2	A_3	A_4	Knob angle	Force
0.075	0.831	0.2578	0.5184	0.9136	10	1
0.074	0.8320	0.2630	0.4980	0.9371	10	0.9867
0.075	0.828	0.2697	0.4835	0.9543	10	0.9726
0.080	0.8189	0.2901	0.4415	0.4415	10	0.9725
0.073	0.8329	0.2634	0.4958	0.9346	10	0.9379

estimated contact forces are compared to the real values in Fig. 23(b) for unseen testing data set. In this figure, the red dash line ($y = x$) is the real force in which the estimated values near the line are more accurate and the residual of regression is smaller. Regression loss of absolute error is between 0.0016 N to 0.059 N where tip contact force values are from 0.16 N to 0.275 N, as tabulated in table 4. Achieved error confirms the effectiveness of the learning model. Fig. 23(a) demonstrates the estimation error of the model as a percentage to the true values. Positive error is an over-estimated value, and negative is an underestimated value. Estimation error of less than 4% is achieved, which validates model in force estimation for unseen catheter tip section shape. The computed mean-absolute-error (MAE) of the estimated force in reference to real force was 0.042 N.

The estimated forces do not follow a consistent underestimation or over-estimation trend, which suggests that the proposed methodology sources no systematic error. Estimation accuracy is likely dependent on how well the learning regression model fitted to the data. Additionally, the noise error is due to the force/torque sensor (ATI Mini 40-E transducer), image processing, camera, or other variations in data collection. Another source of the error might be because of an inappropriate curve-fitting over the catheter. As it can be seen in Fig. 24, the model can not observe catheter's shapes because of the states at 15, 40, 100, and 170.

Table 4: Tip contact force range and regression error.

Contact Force (N)			Metrics		
Min	Max	Avg	Min Error	Max Error	MAE
0.160	0.275	0.218	0.0016	0.059	0.042

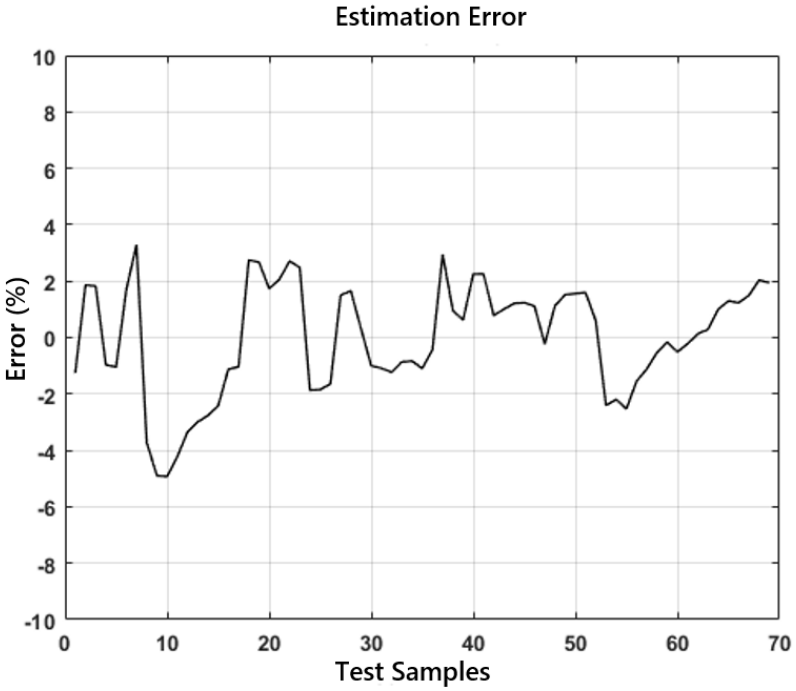

(a)

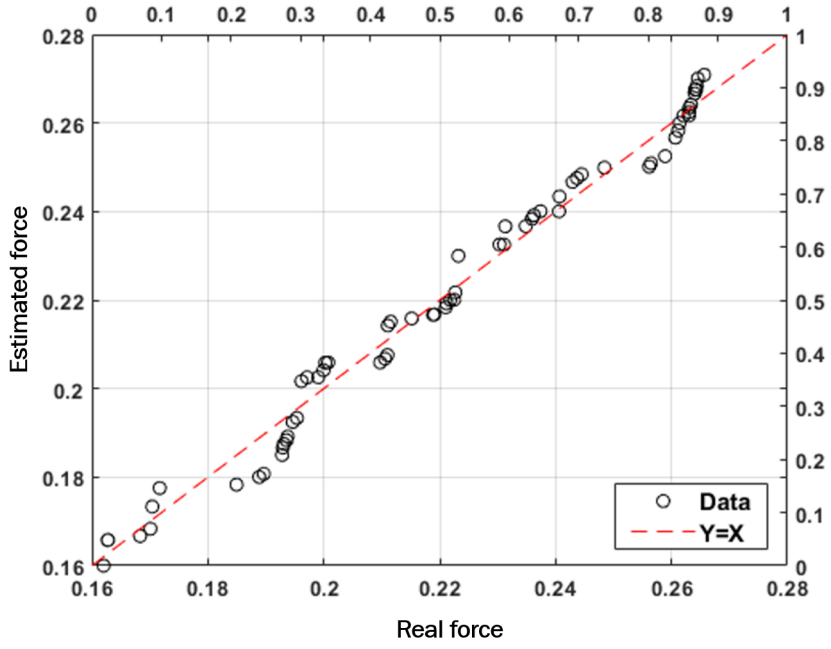

(b)

Figure 23: (a) Estimation error for unseen testing data set, (b) estimated catheter tip contact forces for unseen testing data set are compared to the real force measurements.

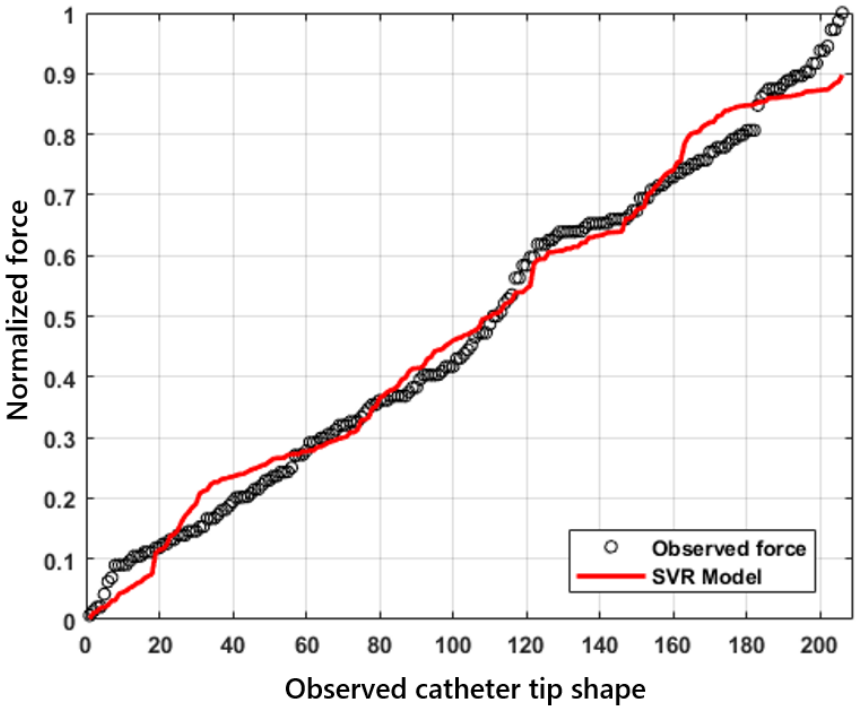

Figure 24: SVR model fitted to the observed training data set.

Chapter 4

A Deep-Learning Force Estimator System for Intracardiac Catheters

4.1 Introduction

Cardiovascular diseases (CVDs) have become a leading problem of mortality across the world with a current number of 17.3 million deaths throughout a year, and it is expected to increase by up to 23.6 million deaths by the year 2030, depicting 31 percent of all global mortalities [131]. Most significantly, cardiovascular diseases risk factors could contribute to cardiac structural changes that are closely associated with electrical disruption and cause of arrhythmia [12]. Cardiac electrical disruption usually causes arrhythmia involving changes in heart rates, irregular beats, and atrial fibrillation. Arrhythmia leads to uncoordinated contractions and relaxations in various regions of the myocardium, that can be supraventricular (e.g., atrial fibrillation) or ventricular [10]. Treatment of arrhythmia goes into two categories; Pharmacological and Non-pharmacological therapeutic options, anti-arrhythmic drugs (AAD) are the primary treatment for rate control in the most extensive patients with Atrial Fibrillation (AF). In contrast, ablation of the AV conduction system is an alternative that often results in extraordinary symptomatic remedy[132].

Throughout the ablation procedure, the catheter is directed into the vasculature and placed inside the heart to deliver heating energy to ablate some portions of cardiac tissue. Ablation procedure has revolutionized the treatment of cardiovascular diseases, and it is considered standard practice in such treatments. Unlike conventional open-heart surgery, the minimally invasive catheter ablation considerably carries less injury due to the small slash size of catheter insertion. It entails less discomfort and rapid discharge of the patients. According to the studies and Meta-analysis done between years 1989 and 1998 that over a total of 1181 patients underwent Radio-frequency ablation (RFA); it was achieved that AV nodal ablation remarkably recovered cardiac symptoms, quality of life, and healthcare utilization for patients with symptomatic AF refractory to AAD [133]. Radio-frequency ablation corrects the electrical signals heart pathway and terminates the arrhythmia.

Minimally invasive catheter ablation procedures comprise various advantages, i.e., minimal incisions, fast recovery time, less bleeding, and is considered as a cost-effective treatment Though, minimally invasive surgery therapy (MIST) has provided many benefits to medical societies but conventional ablation procedures are lacking the force and tactile feedback that may create complications in the treatment. The effective range of tissue-contact force at the tip of ablation catheters is $0.1N$ to $0.3N$[95]. In the sense that applying excessive force in steering the catheters by the surgeon might damage the heart tissue and subsequently inadequate force might cause a deficient ablation treatment [66].

With the aim of reducing radiation from X-Ray fluoroscope to surgeons and patinas during catheterization and dexterity in the interventions, Robot-assisted minimally invasive surgery (RMIS) was developed and emerged to hold this promise for developing the efficiency and skill of surgeons while minimizing injury to the patients. Besides, the interventionists and staff benefit from its excellent visual feedback such as Sensei™ robotics catheter system and Niobe™ magnetic catheter navigation system. Robot-assisted minimally invasive surgery (RMIS) are categorized in three main

divisions: electrophysiologic intervention (EPI), percutaneous coronary intervention (PCI), percutaneous peripheral intervention (PPI). Radio-frequency ablation is placed under umbrella of EPI procedure. The electrophysiology (EP) study uses the imagery to evaluate the origin of the arrhythmia.

The catheters equipped with electrodes at the pointers can convey electrical pulses to the heart and record the heart's electrical activities. When EP recognizes a specific heart tissue causing the arrhythmia, the surgeon will locate the ablation catheter tip at the area of the irregular heart tissue to create a scar/damage in the tissue that probably brings about arrhythmia. Radio-frequency ablation corrects the electrical signals heart pathway and terminates the arrhythmia.

Widespread clinical achievement with RMIS has been negligible. However, still this system suffers the shortage of haptic (force and tactile) feedback given to the surgeon is a limiting factor and reduces the efficiency [134]. In minimally invasive surgery (MIS), surgeons indirectly sense the instrument's interaction with the heart tissue through a long shaft, which kills tactile and forces signals. Based on the studies done, the loss of force feedback in MIS has led to intra-operative injury [135]. In teleoperated robot-assisted minimally invasive surgery (RMIS), all-natural haptic feedback is excluded. The surgeon has no longer control over the manipulation of the instrument directly.

The researches on force analysis approaches at the catheter tip fall into two categories: sensor-less methods (Estimation) and embedded force sensing elements (Measurement). One of the sensor-based approaches to measure the tissue-contact force in MIS is the implementation of a standard sensor to a modified trocar outside the patient that provides a smooth measurement of manipulation of force [136]. Following that, the alternative approaches are proposed such as audio feedback [137], graphical feedback [138], vibrotactile display that is the other form of hepatic feedback [139] and also some other examples of tactile sensors include piezoelectric arrays [140], capacitive sensors [141], force-sensitive resistors [139] and Fiber Bragg Grating FBG [142]

which are mainly embedded in ablation catheters tip to estimate the force directly. Shape estimation of the ablation catheter using two electromagnetic sensors and designing a kinematic redundancy manipulator of the catheter model could estimate the force at points or multiple points[108]. Although, the structures of catheters equipped with force sensors are complicated by far and reduce the reliability and deliverability [105]. Furthermore, catheters size limit and sterilizability of sensors implemented at tip of ablation catheters can be taken as a critical matter [106]. In addition, during catheterization, visualizing the patient's anatomy plays a significant role and most likely X-ray fluoroscopy and MRI are used. MRI is a compatible solution but it affects the functionality of embedded-sensor catheter ablations [103]. X-ray fluoroscopy imaging is source of radiation and interventionists and staff may be exposed to the scattered radiation which extremely affects their health in the long term [7][93]. Thus, model-based force estimation is considered as an alternative approach to accomplish the task. Sensor-less approaches suggest that the force estimation at catheter tip can be gained by changes in catheter's shape/position and orientation of the distal shaft [111]. Another approach is catheter model-based force estimation; this method can estimate the force according to the pose analysis of the catheter tip and the identified parameters of the elastic model of ablation catheters [143]. Predictive modeling for microwave ablation procedure has been developed to estimate the catheter contact force. In this work, we devised a solution based on a deep learning method to address the problem of contact force estimation at catheter tip (Fig. 25).

As a sensor-less solution, the system is directly fed by the data emitted from a camera. The camera plays the role of X-Ray imaging in the authentic operation room. It provides the model with the successive images of the catheter. The model estimates applied forces to the catheter using the corresponding deflection of the shape. This system can overcome the difficulties that embedded-sensor catheters may be involved; besides the accuracy and robustness of this technique are of great importance in real-time applications. This technique relies on learning the images

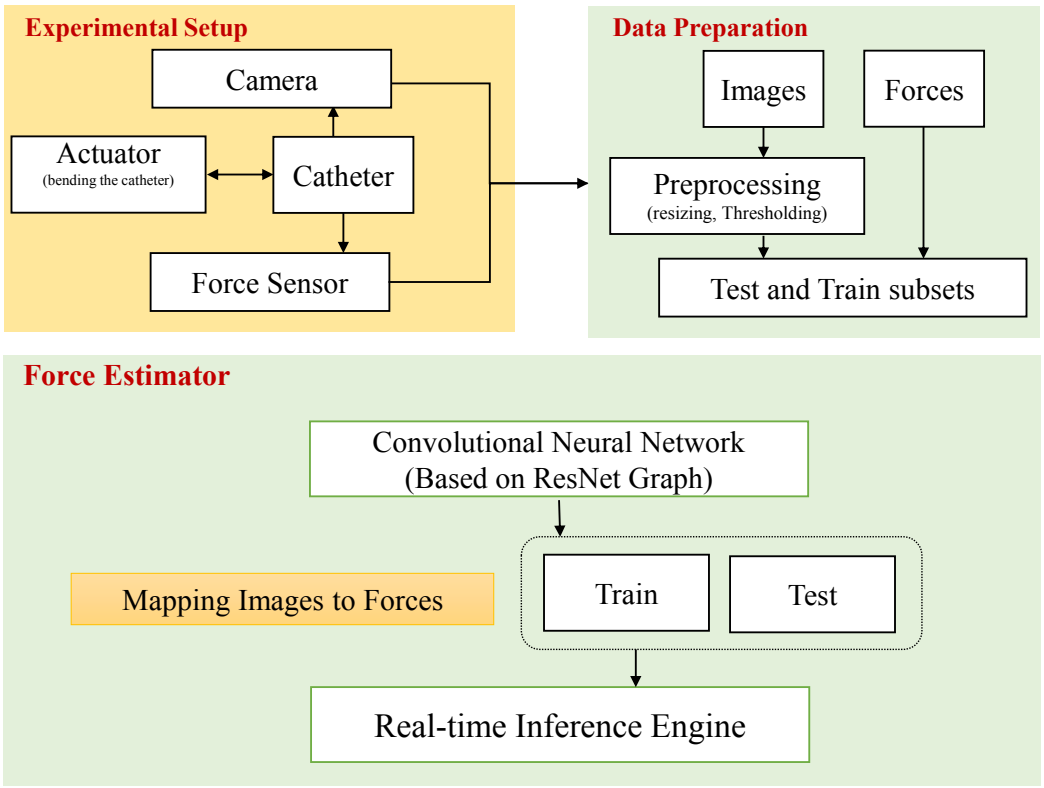

Figure 25: This diagram shows the general architecture of the proposed method.

of the distal section of catheters and estimation of the force corresponding to those images. During the catheterization, the surgeon is able to control the force using the estimated force acquired from the generated model. In contrast to the methods that employ a feature extraction phase before the learning phase, the proposed solution elicits essential features and trains the model simultaneously. In other words, the system aims to solve a regression problem in such a way that maps the input images to the 2D dimensional space of forces. It trains the model through an end-to-end network. Having the catheter images during the surgery, the system can approximate forces in two directions.

To collect data, a test setup is designed to simulate ablation procedure and catheter deflection from insertion vein femoral (Fig. 21) in interaction with artificial heart tissue. The setup includes a 2-DOF heart simulator to resemble the heart motion and drives the deflection while the catheter tip contacts the tissue. We record

the contact forces using a 6-DOF force/torque sensor mounted at the artificial tissue and capturing images of the shape of the distal catheter section with a camera. Having generated the mathematical model, it will be used to predict the contact forces based on the catheter images and catheter knob angles to evaluate the model validity.

The main contributions of the proposed solution are listed as follows: it is not required to perform a series of specific complicated preprocessing operations for compiling the input data. Besides, the system is capable of making decisions on every image without exerting either mathematical or machine vision-based algorithms for feature extraction. For example, some literature methods calculate the mathematical characteristics of the catheter's inflection to approach a correct definition of the shape. However, these kinds of methods are chiefly incapable of modeling the curves, which are not defined in a mathematical function format. The trained model is also invariant to translation, scaling, and rotation so that the force can be attained regardless of the curvature's degree. For the sake of simplicity, we call the proposed method Deep Catheter Force Estimator (DCFE).

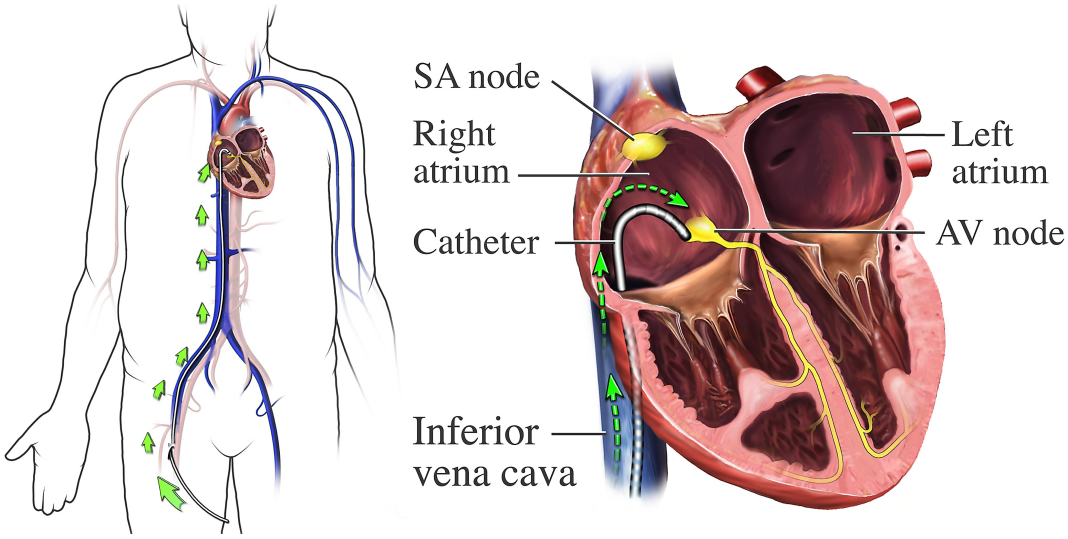

Figure 26: Sample of cardiac ablation catheter insertion path from femoral access.

4.2 Experimental setup and procedure

4.2.1 Experimental setup

The experimental setup was designed to simulate the insertion area, path and deflection in catheter during ablation therapy in heart chamber to collect force data at the catheter tip. To reproduce the heart motion, a heart simulator was sat up.

The setup is presented in Fig. 27 and consists of catheter contact force measurement platform, motion simulator, camera, Boston Scientific Blazer II XP Temperature Ablation catheter, guide sheath and adjustable holders/fixtures. As shown in Fig. 28, the heart motion simulator has two linear actuators that are equipped with stepper motors (17HS4401-S 40 mm Nema) powered by HANPOSE TB660. Those two linear actuators are perpendicularly assembled to simulate the heart's two-DOF-motion. A six-axis force-torque sensor (ATI mini 40-E transducer) was mounted on the heart simulator to measure force when the catheter is in contact with an artificial tissue. The artificial heart tissue is fixed on the F/T sensor to produce the interaction between soft catheter and tissue. Fig .26 depicts the catheter path from femoral access. A sheath and adjustable holders in our setup create a similar path, which catheter goes through it (Fig. 27).

4.2.2 Data preparation

Initially, to collect the force data corresponding to catheter deflection, the catheter knob was fixed at the degree of 10. The heart simulator starts moving in a sinusoidal forward-lateral motion. Simultaneously, the catheter tip remains in contact with artificial tissue mounted on the heart simulator. The camera was implemented perpendicularly on the contact location of the catheter and moving artificial heart tissue, and tracking tip deflection under 2D. The camera captures the deflected tip section's images with a sampling rate of 24 HZ, following that a six-degree-of-freedom

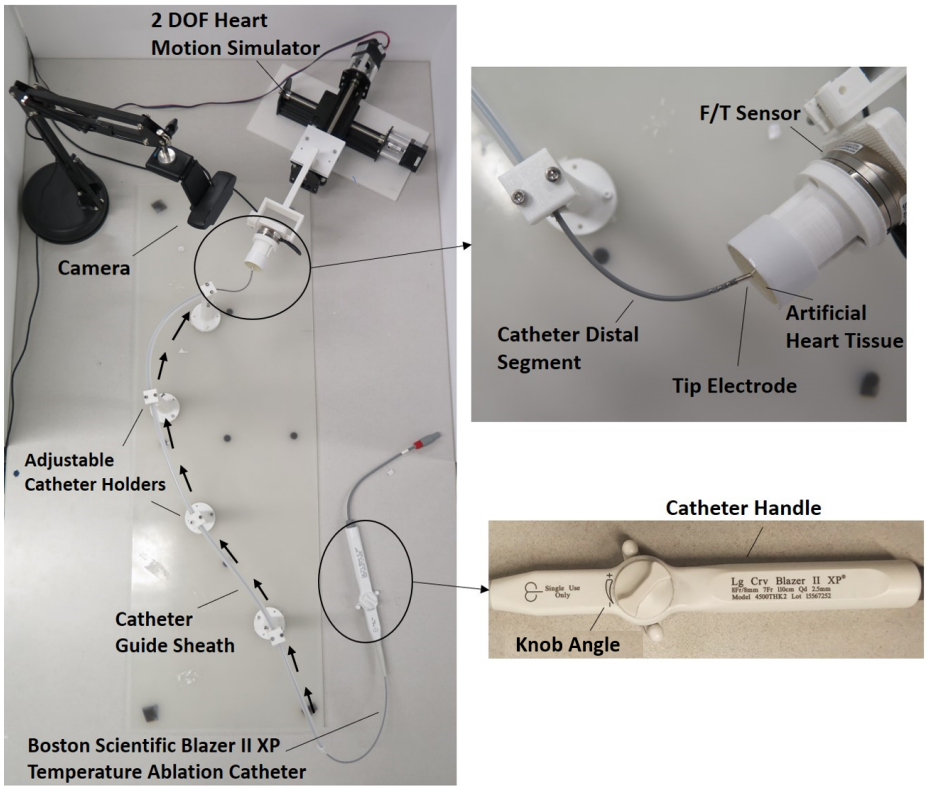

Figure 27: Experimental test setup simulates catheter tip in contact with heart tissue during ablation therapy.

force-torque sensor (ATI mini40-E transducer) begins recording the force of contacting the catheter tip with artificial heart tissue simultaneously. In this experiment, we implemented our module on Python using tensor flow 2.0.

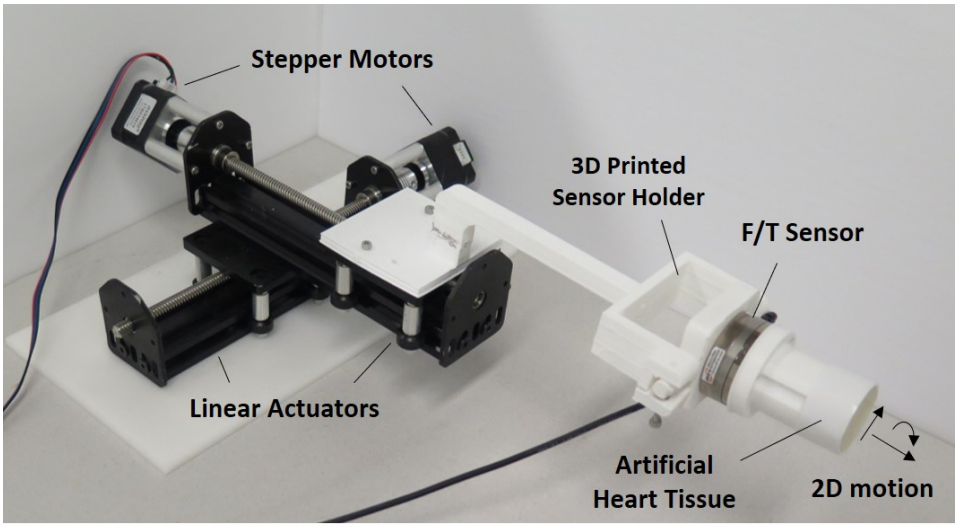

Figure 28: 2 DOF heart simulator equipped with F/T transducer and artificial tissue.

Figure 29: The diagram demonstrates the architecture of the DCFE, which is designed based on the Resnet graph [48].

The following step is generating the convolutional neural network (CNN) by training the DCFE, including the images of the catheter, corresponding forces as features, and labels. Our data set is categorized into 154 testing samples and 461 training samples to evaluate the validity of the convolutional neural network (CNN) and estimate the force in a real-time platform (Fig. 25)

4.3 Methodology

As mentioned in the previous section, the proposed method attempts to translate the images of catheters into the force space and provide surgeons with a tangible estimation of applied forces. Hence, an experimental setup has been utilized with the intention of simulating the actual therapy with common equipment for a specific catheter ablation task. In a real case, the surgery is accomplished under the X-ray fluoroscopy imaging and a surgeon corrects the trajectory by referring to the real-time imaging mechanism. Similarly, the setup encompasses a camera to capture the images from catheter's motions, while an actuator is driving the tip within an artificial plastic vein and squeezing it on a force sensor. The collected data is then used to train a deep learning model.

A Convolutional Neural Network (CNN) is considered as a feature extractor and also a regression analyzer for acquiring a robust model on the given data set. Since the temporal behavior of the data is not supposed to be investigated, a feed-forward deep learning model based on the ResNet architecture is employed [48]. The graph of the neural network is modified in such a way that it receives 2D images with RGB channels in the input and generates a 2D vector corresponding to every input image as the estimated force x and y (Fig. 29).

Deep convolutional neural networks are mainly used to process the image data. stacked layers constitute the graph of an end-to-end sub-network. It widely performs not only as a feature extractor in a deep object detector, but also as a classifier

in object recognition problems [144, 145]. On the one hand, it derives the low to high level features from the input image. On the other hand, combining with one or more dense layers, it can discriminate samples' class label or predict target values in the supervised manner.

Moreover, Convolutional neural networks can be enhanced in terms of the performance by revising their graph and number of stacked layers. As a result, increase in the number of layers or making the network deeper leads to achieve a better generalization and outcome in the model. However, it also ends up to some further issues in the design as well. With this in mind, eclectic number of architectures have been proposed to be assessed on challenging datasets such as ImageNet [146]. For instant, the mostly referred and popular CNNs such as LeNet, VGG-16, AlexNet and ResNet have been introduced with a particular design [47, 46, 147, 48]. Every intended architecture follows a specific mechanism to improve the performance of the final model, thereby extracting highly robust features.

As mentioned earlier, ResNet is the preferred architecture for the proposed method. To this end, we more concentrates on the internal structure of this network, in spite of inordinate precious sources in the literature [48]. Basically, the DNN is supposed to receive the input image $\tau \in R^{n \times n}$ and projects it to the output $\gamma \in R^2$, where n is the dimension of the input image and γ is the forces in a 2D space x and y.

$$\gamma_i^l = F(\tau_i^l) \tag{16}$$

where i is the number of input sample and l denotes the layer's number. Normally, a 2D convolution layer followed by a pooling layer and a specific activation function constitutes a full layer in CNNs. Stacking several layers of this kind make a deeper networks. The parameters of the network should be regulated using Stochastic Gradient Decent (SGD) and back propagation method. Although the deep network increases the accuracy of models, vanishing gradient causes the degradation problem in the

optimization. As a solution, ResNet has been introduced with the aim of enabling DNNs to have a deeper graph without encountering with vanishing gradient problem. ResNet utilizes the residual mapping for approximating the input in such a way that the process is done through the residual function $H(\tau_i^l)$ rather than the function (1):

$$H(\tau_i^l) = \sigma(F(\tau_i^l) + \tau_i^l) \tag{17}$$

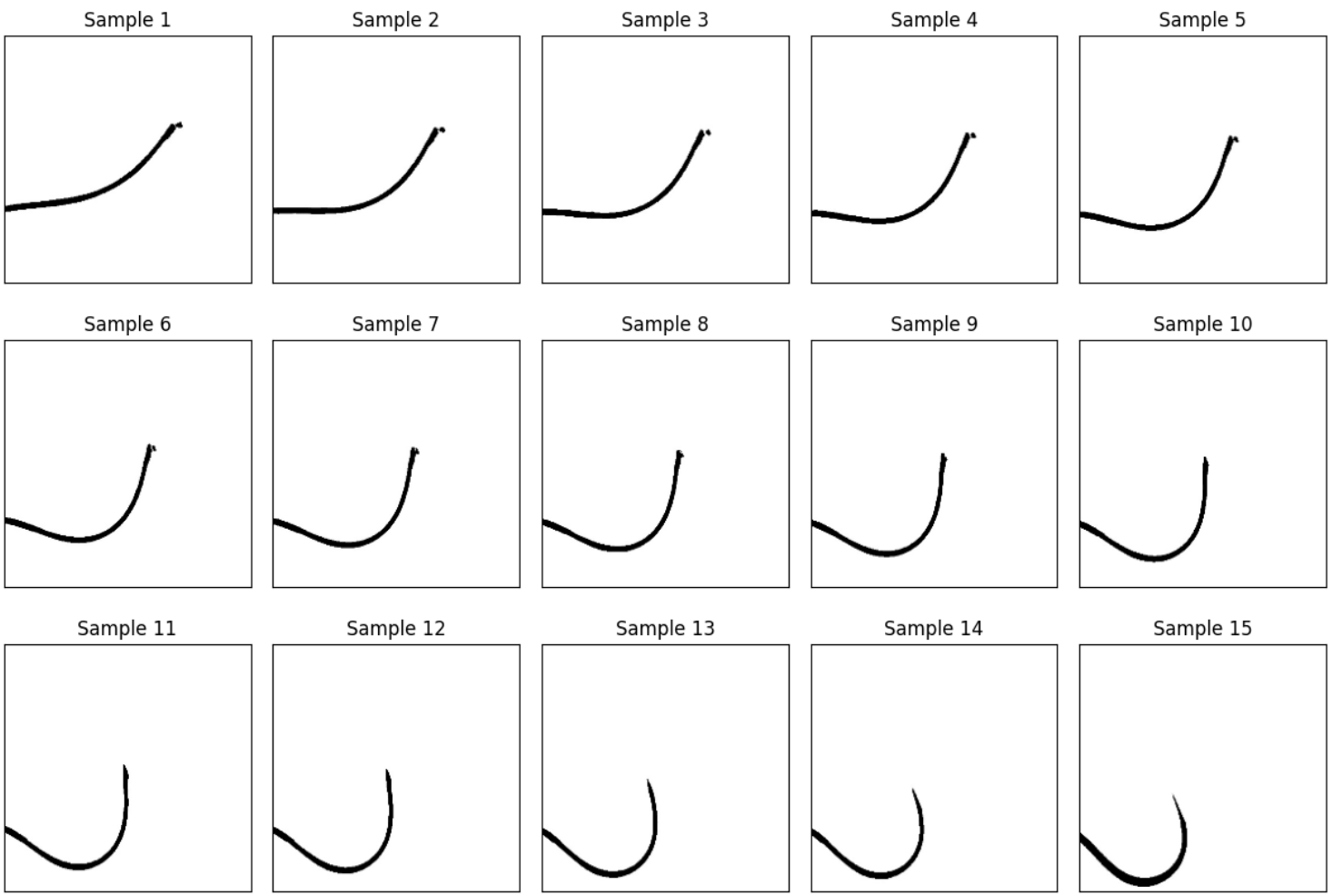

Figure 30: The diagram shows the images of the catheter captured from the designed setup. Here is a set of sample images that used to evaluate the model.

where $F(\tau_i^l)$ points to a residual block including convolution and batch normalization layers and also, σ denotes the corresponding activation function. Our proposed solution uses ResNet-18 as the desired architecture for CNN (see Fig. 5). In order to estimate forces in the 2D directions, a dense layer is added to the last layer of the graph as follows:

$$\gamma^l = WF(\tau_i^l) + b \tag{18}$$

where l here is the output layer and W and b are weights and biases respectively. Also, the loss function below is utilized so as to train the model as well as evaluate the performance:

$$loss(r, p) = \sqrt{\frac{\sum_{i=1}^{d}(r_i - p_i)^2}{d}} \tag{19}$$

Obviously, r denotes the real forces and p is the predicted values in $d = 2$ dimensions. The graph is optimized using the above function in a supervised manner. Using the aforesaid architecture, it is conceivable to extract the relationship between every input image and its corresponding force vector.

4.4 Evaluation and Discussion

As mentioned before, DCFE's graph has been designed based on the ResNet architecture. Fig. 29 shows the designed diagram of the CNN. An input image goes through a 2D convolution layer with 64 filters of size 7×7, followed by a batch normalization layer and Relu activation function. A 3×3 max-pooling operator is applied to the output of the Relu. Afterward, the output traverses four successive residual blocks with 64, 128, 265, and 512 filters. Every residual block itself comprises convolution and batch normalization layers. A fully connected layer with two neurons is then fed by the output of the last residual layer. This layer plays the role of regression in order to map the feature maps of the CNN to desired forces in the x and y direction.

The DCFE was fed by the catheter's images captured from the setup for both training and evaluating purposes. Each image was resized to a $224 \times 224 \times 3$ tensor. Afterward, every pixel was normalized to have a value between 0 and 1. Fig. 30 demonstrates some samples of images used for the test phase of the model. A data set was generated using the forces in the x and y direction associated with preprocessed images. In contrast to the image data, the forces' values were not normalized so that the

Table 5: Performance of the model. Min, Max and RMSE estimation errors are tabulated.

Force Direction	Min Error	Max Error	RMSE
x	0.0001	0.066	0.028
y	0.0003	0.068	0.023

DCFE would provide predictions on the actual forces. The dataset was divided into 461 training and 154 testing samples. The DCFE was trained in 10000 epochs on the training set to translate every input image into the corresponding forces in the x and y directions. In fact, the DCFE deploys a regression to estimate the forces' actual values using images of the catheters. Furthermore, the DCFE was evaluated on unseen images of the test set, as shown in Table 1. This table reports the RMSE and the minimum and maximum errors of the model's prediction on the x and y. To be more precise, the trained model was loaded to the inference engine to predict the forces using input images. It is worth saying that designing and training the model and building the inference engine were implemented in Python using TensorFlow 2.0 [148].

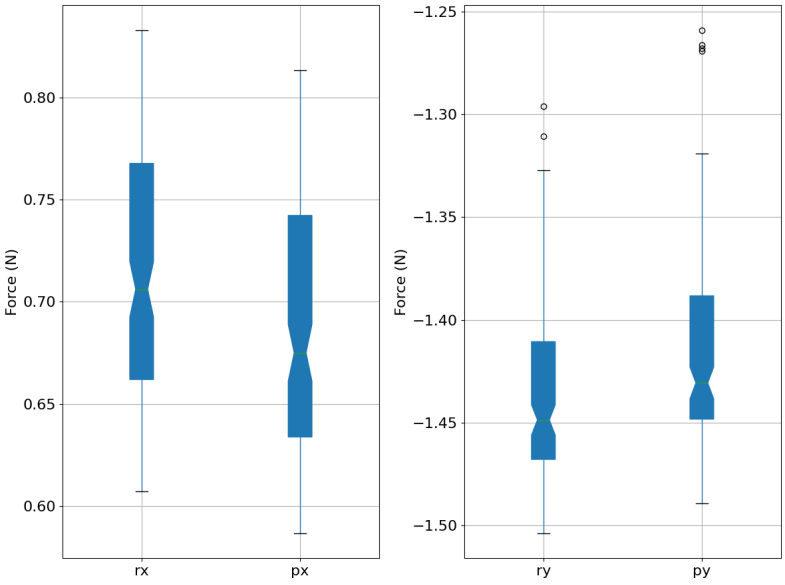

Figure 31: The diagram illustrates the distribution of both actual and predicted force in the x and y direction. rx and ry are the real force data while px and py are the predicted values. the plot provides the minimum, maximum, median, quartiles and outliers of the data.

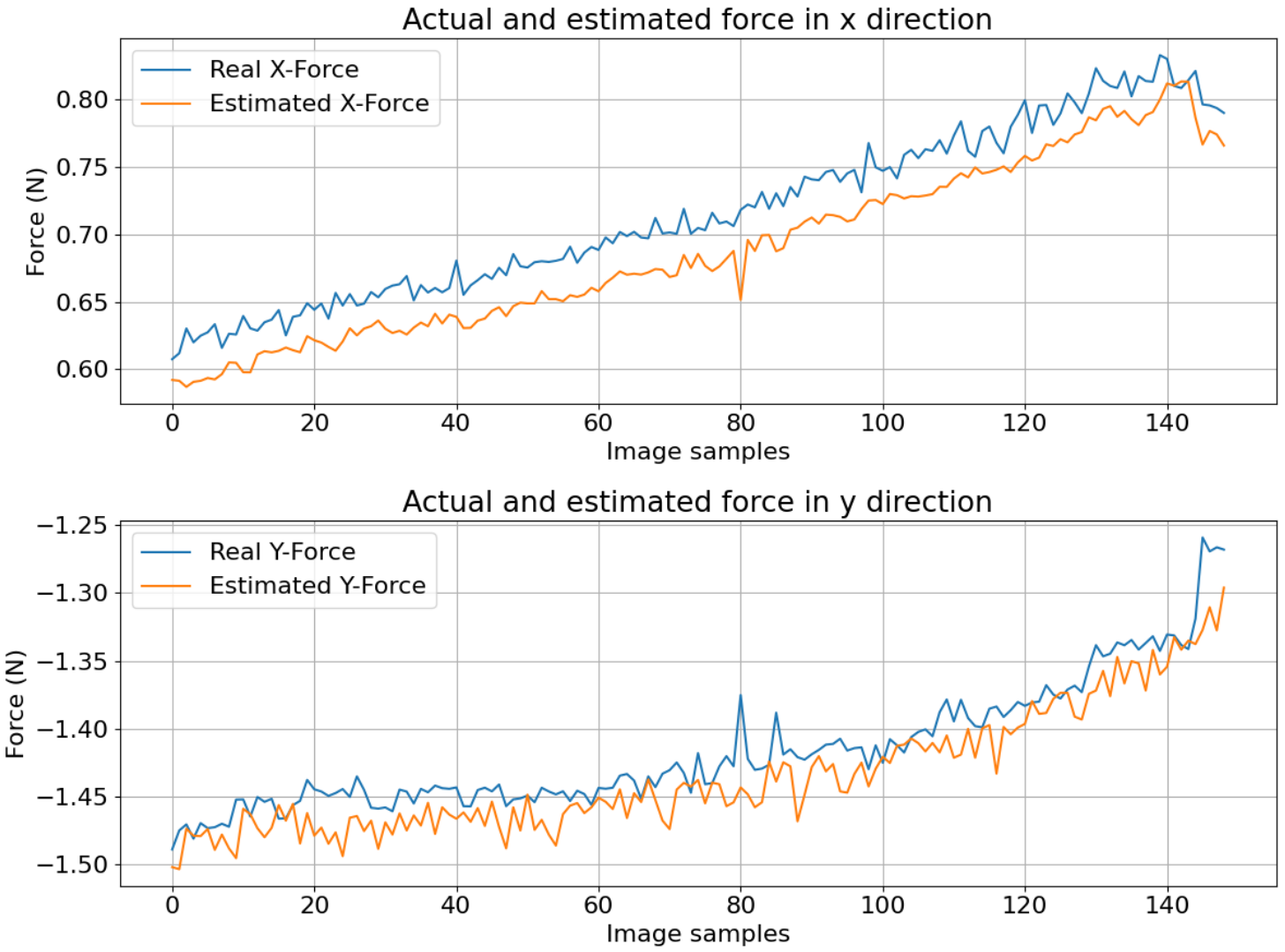

Figure 32: The graphs depict the model performance using its estimations on 154 catheter's images from the test dataset.

Fig. 31 displays the variation of both actual force data and the predicted result. The left subplot shows the minimum, maximum, median, quartiles, and outliers of the data, as mentioned earlier, for forces in the x-direction (rx and px). The right subplot provides that information for the forces in the y-direction (ry and py).

As mentioned earlier, either of real and estimated forces has not been normalized, so the distribution in the Fig. 31 is scattered based on the actual values. Although the results of x and y have been investigated separately, the DCFE makes predictions on both directions simultaneously. In other words, the last fully-connected layer in the graph contains two neurons for mapping to the output size.

Fig. 32 depicts the performance of the DCFE in estimating the forces. The top subplot provides the estimated and actual force values in the x-direction in orange and blue respectively. The bottom subplot gives the results of the model compared with the real target of forces in the y-direction. As shown in the plots, the model was successfully trained on the given dataset and provided reasonable predictions with an acceptable accuracy on the test images. Using the capability of deep learning, the model was able to process the input images without further preprocessing and feature extraction. The model addresses the problem of force estimation for catheters with a robust sensor-less solution, in which it only utilizes the data captured by a camera.

Chapter 5

Conclusion and Future Work

5.1 Conclusion

The use of the ablation catheters with the sensor at tip carries complications, such as high cost, error in the force measurement accuracy from nearby ferrous materials, less deliverability, and steerability. The objective of this work was to develop and experimentally validate a learning-based predictive method for catheter tip contact force using imaging data. The predictive force model is generated using the support vector regression algorithm. The polynomial coefficient of a curve fitted to deflected catheter tip shape and knob actuation angle features and contact force are considered targets. The proposed learning solution is originated from the fact that expert clinicians control tip contact force through visual learning of the tip shape. The observed shape and the force of a catheter tip in contact with an artificial tissue were collected in our test setup with a 2D heart motion simulator and an ablation catheter in a path from femoral access to the heart chamber. The predictive model yielded catheter tip force estimation in close agreement with actual values for unseen data. An absolute error of less than 0.059 N (within range of 4%) was achieved. A further step is vital to implement the method in clinical ablation treatment. The learning-based force estimation is an advancement toward automated robotic ablation therapies. Force

prediction solutions can be developed for other cardiovascular procedures and instruments based on the proposed approach.

Furthermore, the deep learning-based method was presented for estimating the generated force directly from the catheter images. It aims to deliver insight into catheter-heart tissue interaction forces. It improves surgeons' performance as well as the reliability of ablation treatments of cardiovascular diseases. The proposed solution is considered a sensor-free method in such a way that it only utilizes the data that emerged from the common equipment in operation rooms. In other words, the model maps input images to their corresponding forces in the x and y-direction. Regardless of how complicated is Catheter deflected shape, the model can predict the force with reasonable precision. Moreover, the proposed method is fed by raw images without performing feature extraction operations. A mechanical setup was designed and made to physically simulate ablation therapy and collect force-image data. Finally, the method was assessed by the unseen data, and the result showed that the trained model could effectively estimate the force.

5.1.1 Future Work

As future works, the proposed method can be developed in methodology and practice. Experimentally, a significant problem in both robotics-assisted invasive surgery and invasive manual surgery is controlling the catheter-tissue contact force. Robots and surgeons are subjected to catheter-tissue contact forces whenever they perform tasks, including motion constrained by the heart tissue. To control the catheter-tissue contact force, a control system can be added to the deep neural network (DNN) model for enhancing the performance of robotic minimally invasive surgery (RMIS). In other words, force control plays a vital role in minimally invasive surgeries; thus, the proposed method can be considered a feedback element in the force control system (Fig. 33). The suggested method can also be implemented on other types of interventional

devices and cardiovascular procedures to develop image-based sensing solutions in a real-time platform. Estimating the three dimensions of the contact force using the DNN model can also be considered potential future research. Validating the method in a clinical condition under fluoroscopy imaging is an intuitive step. Besides, enriching the proposed system to map images to the force space to become more precise is taken into the future step.

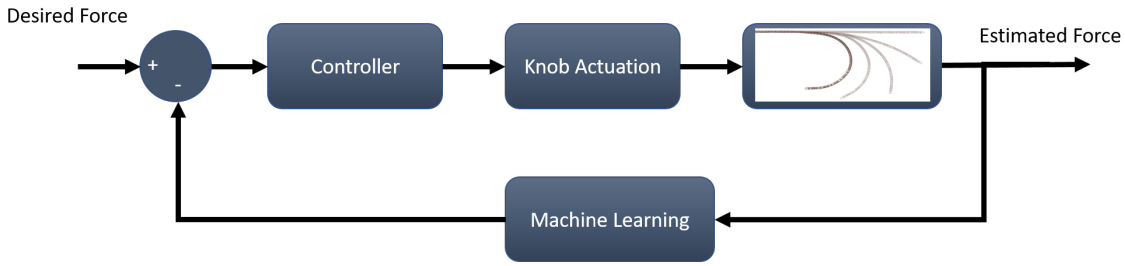

Figure 33: Closed-Loop force control using machine learning model as feedback element.

Bibliography

[1] Shorya Awtar, Tristan T Trutna, Jens M Nielsen, Rosa Abani, and James Geiger. Flexdex™: a minimally invasive surgical tool with enhanced dexterity and intuitive control. *Journal of Medical Devices*, 4(3), 2010.

[2] TG Frank, GB Hanna, and A Cuschieri. Technological aspects of minimal access surgery. *Proceedings of the Institution of Mechanical Engineers, Part H: Journal of Engineering in Medicine*, 211(2):129–144, 1997.

[3] Minoru Tabata, Ramanan Umakanthan, Lawrence H Cohn, Ralph Morton Bolman III, Prem S Shekar, Frederick Y Chen, Gregory S Couper, and Sary F Aranki. Early and late outcomes of 1000 minimally invasive aortic valve operations. *European journal of cardio-thoracic surgery*, 33(4):537–541, 2008.

[4] James L Cox. Cardiac surgery for arrhythmias. *Pacing and clinical electrophysiology*, 27(2):266–282, 2004.

[5] Han-Shiang Chen and Shyr-Ming Sheen-Chen. Synchronous and "early" metachronous colorectal adenocarcinoma. *Diseases of the colon & rectum*, 43(8):1093–1099, 2000.

[6] Shahir. Hasanzadeh. Modeling, force estimation and control of steerable catheters for robot-assisted intra-cardiac navigation. In *A dissertation presented to Ryerson University*, pages 1–7, 2016.

[7] Mohammad Ali Tavallaei, Daniel Gelman, Michael Konstantine Lavdas, Allan C Skanes, Douglas L Jones, Jeffrey S Bax, and Maria Drangova. Design, development and evaluation of a compact telerobotic catheter navigation system. *The International Journal of Medical Robotics and Computer Assisted Surgery*, 12(3):442–452, 2016.

[8] Amir Hooshiar, Siamak Najarian, and Javad Dargahi. Haptic telerobotic cardiovascular intervention: a review of approaches, methods, and future perspectives. *IEEE Reviews in Biomedical Engineering*, 13:32–50, 2019.

[9] Arthur Keith and Martin Flack. The form and nature of the muscular connections between the primary divisions of the vertebrate heart. *Journal of anatomy and physiology*, 41(Pt 3):172, 1907.

[10] Lukas J Motloch and Fadi G Akar. Gene therapy to restore electrophysiological function in heart failure. *Expert opinion on biological therapy*, 15(6):803–817, 2015.

[11] Dariush Mozaffarian, Emelia J Benjamin, Alan S Go, and Arnett. Executive summary: heart disease and stroke statistics—2016 update: a report from the american heart association. *Circulation*, 133(4):447–454, 2016.

[12] André G Kléber and Yoram Rudy. Basic mechanisms of cardiac impulse propagation and associated arrhythmias. *Physiological reviews*, 84(2):431–488, 2004.

[13] Gregory YH Lip, Frank R Heinzel, Fiorenzo Gaita, Jose Rámon Gonzalez Juanatey, and Le Heuzey. European heart rhythm association/heart failure association joint consensus document on arrhythmias in heart failure, endorsed by the heart rhythm society and the asia pacific heart rhythm society. *Ep Europace*, 18(1):12–36, 2016.

[14] Stanley Nattel. New ideas about atrial fibrillation 50 years on. *Nature*, 415(6868):219–226, 2002.

[15] Alan S Go, Elaine M Hylek, and Phillips. Prevalence of diagnosed atrial fibrillation in adults: national implications for rhythm management and stroke prevention: the anticoagulation and risk factors in atrial fibrillation (atria) study. *Jama*, 285(18):2370–2375, 2001.

[16] DG Wyse. Atrial fibrillation follow-up investigation of rhythm management (affirm) investigators: A comparison of rate control and rhythm control in patients with atrial fibrillation. *N Engl J Med*, 347:1825–1833, 2002.

[17] Nassir F Marrouche, Thomas Dresing, Christopher Cole, Dianna Bash, Eduardo Saad, Krzysztof Balaban, Stephen V Pavia, and Schweikert. Circular mapping and ablation of thepulmonary vein for treatment of atrial fibrillation: Impact of different catheter technologies. *Journal of the American College of Cardiology*, 40(3):464–474, 2002.

[18] Hein JJ Wellens. Catheter ablation of cardiac arrhythmias: usually cure, but complications may occur, 1999.

[19] Giuseppe Stabile, Emanuele Bertaglia, Gaetano Senatore, Antonio De Simone, Francesca Zerbo, Giovanni Carreras, Pietro Turco, Pietro Pascotto, and Massimo Fazzari. Feasibility of pulmonary vein ostia radiofrequency ablation in patients with atrial fibrillation: a multicenter study (cacaf pilot study). *Pacing and clinical electrophysiology*, 26(1p2):284–287, 2003.

[20] Hugh Calkins, Matthew R Reynolds, Peter Spector, Manu Sondhi, Yingxin Xu, Amber Martin, Catherine J Williams, and Isabella Sledge. Treatment of atrial fibrillation with antiarrhythmic drugs or radiofrequency ablation: two systematic literature reviews and meta-analyses. *Circulation: Arrhythmia and Electrophysiology*, 2(4):349–361, 2009.

[21] A John Camm, Gregory YH Lip, Raffaele De Caterina, Irene Savelieva, Dan Atar, Stefan H Hohnloser, Gerhard Hindricks, and Paulus Kirchhof. 2012 focused update of the esc guidelines for the management of atrial fibrillation: An update of the 2010 esc guidelines for the management of atrial fibrillation. *Revista Española de Cardiología (English Edition)*, 66(1):54, 2013.

[22] Elena Arbelo, Josep Brugada, Gerhard Hindricks, Aldo P Maggioni, Luigi Tavazzi, and Panos Vardas. The atrial fibrillation ablation pilot study: an european survey on methodology and results of catheter ablation for atrial fibrillation conducted by the european heart rhythm association. *European heart journal*, 35(22):1466–1478, 2014.

[23] Francisco G Cosio, Etienne Aliot, Giovanni Luca Botto, Hein Heidbüchel, Christoph Johan Geller, Paulus Kirchhof, and De Haro. Delayed rhythm control of atrial fibrillation may be a cause of failure to prevent recurrences: reasons for change to active antiarrhythmic treatment at the time of the first detected episode. *Europace*, 10(1):21–27, 2008.

[24] Mohammad Jolaei, Amir Hooshiar, Amir Sayadi, Javad Dargahi, and Muthukumaran Packirisamy. Sensor-free force control of tendon-driven ablation catheters through position control and contact modeling. In *2020 42nd Annual International Conference of the IEEE Engineering in Medicine & Biology Society (EMBC)*, pages 5248–5251. IEEE, 2020.

[25] Andreas Kaplan and Michael Haenlein. Siri, siri, in my hand: Who's the fairest in the land? on the interpretations, illustrations, and implications of artificial intelligence. *Business Horizons*, 62(1):15–25, 2019.

[26] Kevin P Murphy. *Machine learning: a probabilistic perspective*. MIT press, 2012.

[27] Henning Müller, Nicolas Michoux, David Bandon, and Antoine Geissbuhler. A review of content-based image retrieval systems in medical applications—clinical benefits and future directions. *International journal of medical informatics*, 73(1):1–23, 2004.

[28] Christopher M Bishop. *Pattern recognition and machine learning*. springer, 2006.

[29] Maciej Jaworski, Piotr Duda, and Leszek Rutkowski. New splitting criteria for decision trees in stationary data streams. *IEEE transactions on neural networks and learning systems*, 29(6):2516–2529, 2017.

[30] Jürgen Schmidhuber. Deep learning in neural networks: An overview. *Neural networks*, 61:85–117, 2015.

[31] He Yan, Qiaolin Ye, Tian'an Zhang, Dong-Jun Yu, Xia Yuan, Yiqing Xu, and Liyong Fu. Least squares twin bounded support vector machines based on l1-norm distance metric for classification. *Pattern Recognition*, 74:434–447, 2018.

[32] Shichao Zhang, Debo Cheng, Zhenyun Deng, Ming Zong, and Xuelian Deng. A novel knn algorithm with data-driven k parameter computation. *Pattern Recognition Letters*, 109:44–54, 2018.

[33] Deruo. Cheng, Yiqiong . Shi, Tong . Lin, Bah-Hwee. Gwee, and K. Toh. Hybrid K -means clustering and support vector machine method for via and metal line detections in delayered ic images. *IEEE Transactions on Circuits and Systems II: Express Briefs*, 65(12):1849–1853, 2018.

[34] Moloud Abdar, Mariam Zomorodi-Moghadam, Resul Das, and I-Hsien Ting. Performance analysis of classification algorithms on early detection of liver disease. *Expert Systems with Applications*, 67:239–251, 2017.

[35] M Abdar and Mariam Zomorodi-Moghadam. Impact of patients' gender on parkinson's disease using classification algorithms. *Journal of AI and Data Mining*, 6(2):277–285, 2018.

[36] Roohallah Alizadehsani, Moloud Abdar, Seyed Mohammad Jafar Jalali, Mohamad Roshanzamir, Abbas Khosravi, and Saeid Nahavandi. Comparing the performance of feature selection algorithms for wart treatment selection. In *Proceedings of The International Workshop on Future Technology*, pages 6–18, 2019.

[37] Paweł Pławiak. Novel genetic ensembles of classifiers applied to myocardium dysfunction recognition based on ecg signals. *Swarm and evolutionary computation*, 39:192–208, 2018.

[38] Esther E Bron, Marion Smits, Janne M Papma, Rebecca ME Steketee, Rozanna Meijboom, Marius De Groot, John C van Swieten, Wiro J Niessen, and Stefan Klein. Multiparametric computer-aided differential diagnosis of alzheimer's disease and frontotemporal dementia using structural and advanced mri. *European radiology*, 27(8):3372–3382, 2017.

[39] Yann LeCun, Yoshua Bengio, and Geoffrey Hinton. Deep learning. *nature*, 521(7553):436–444, 2015.

[40] David E Rumelhart, Geoffrey E Hinton, and Ronald J Williams. Learning representations by back-propagating errors. *nature*, 323(6088):533–536, 1986.

[41] Md Rishad Ahmed, Yuan Zhang, Zhiquan Feng, Benny Lo, Omer T Inan, and Hongen Liao. Neuroimaging and machine learning for dementia diagnosis: Recent advancements and future prospects. *IEEE reviews in biomedical engineering*, 12:19–33, 2018.

[42] Yann LeCun, Léon Bottou, Yoshua Bengio, and Patrick Haffner. Gradient-based learning applied to document recognition. *Proceedings of the IEEE*, 86(11):2278–2324, 1998.

[43] Paul Smolensky. Information processing in dynamical systems: Foundations of harmony theory (no. cu-cs-321-86). *Colorado Univ at Boulder Dept of Computer Science*, 1986.

[44] Geoffrey E Hinton and Ruslan R Salakhutdinov. Reducing the dimensionality of data with neural networks. *science*, 313(5786):504–507, 2006.

[45] Ronald J Williams and David Zipser. A learning algorithm for continually running fully recurrent neural networks. *Neural computation*, 1(2):270–280, 1989.

[46] Karen. Simonyan and Andrew . Zisserman. Very deep convolutional networks for large-scale image recognition, 2014.

[47] Yann. Lecun, Leon . Bottou, Yoshua . Bengio, and P. Haffner. Gradient-based learning applied to document recognition. *Proceedings of the IEEE*, 86(11):2278–2324, 1998.

[48] Kaiming. He, Xiangyu. Zhang, . Ren, and J. Sun. Deep residual learning for image recognition. In *2016 IEEE Conference on Computer Vision and Pattern Recognition (CVPR)*, pages 770–778, 2016.

[49] Adhish Prasoon, Kersten Petersen, Christian Igel, François Lauze, Erik Dam, and Mads Nielsen. Deep feature learning for knee cartilage segmentation using a triplanar convolutional neural network. In *International conference on medical image computing and computer-assisted intervention*, pages 246–253. Springer, 2013.

[50] Siqi Liu, Sidong Liu, Weidong Cai, Sonia Pujol, Ron Kikinis, and Dagan Feng. Early diagnosis of alzheimer's disease with deep learning. In *2014 IEEE 11th international symposium on biomedical imaging (ISBI)*, pages 1015–1018. IEEE, 2014.

[51] Varun Gulshan, Lily Peng, Marc Coram, Martin C Stumpe, Derek Wu, and Arunachalam Narayanaswamy. Development and validation of a deep learning algorithm for detection of diabetic retinopathy in retinal fundus photographs. *Jama*, 316(22):2402–2410, 2016.

[52] Andre Esteva, Brett Kuprel, Roberto A Novoa, Justin Ko, Susan M Swetter, Helen M Blau, and Sebastian Thrun. Dermatologist-level classification of skin cancer with deep neural networks. *nature*, 542(7639):115–118, 2017.

[53] Shekoofeh Azizi, Sharareh Bayat, Pingkun Yan, and Amir Tahmasebi. Detection and grading of prostate cancer using temporal enhanced ultrasound: combining deep neural networks and tissue mimicking simulations. *International journal of computer assisted radiology and surgery*, 12(8):1293–1305, 2017.

[54] Jun Shi, Shichong Zhou, Xiao Liu, Qi Zhang, Minhua Lu, and Tianfu Wang. Stacked deep polynomial network based representation learning for tumor classification with small ultrasound image dataset. *Neurocomputing*, 194:87–94, 2016.

[55] Qi Zhang, Yang Xiao, Wei Dai, Jingfeng Suo, Congzhi Wang, Jun Shi, and Hairong Zheng. Deep learning based classification of breast tumors with shear-wave elastography. *Ultrasonics*, 72:150–157, 2016.

[56] U Rajendra Acharya, Hamido Fujita, Shu Lih Oh, Yuki Hagiwara, Jen Hong Tan, and Muhammad Adam. Application of deep convolutional neural network for automated detection of myocardial infarction using ecg signals. *Information Sciences*, 415:190–198, 2017.

[57] Jonathan Rubin, Rui Abreu, Anurag Ganguli, Saigopal Nelaturi, Ion Matei, and Kumar Sricharan. Recognizing abnormal heart sounds using deep learning. *arXiv preprint arXiv:1707.04642*, 2017.

[58] Majd Zreik, Nikolas Lessmann, Robbert W van Hamersvelt, Jelmer M Wolterink, Michiel Voskuil, Max A Viergever, Tim Leiner, and Ivana Išgum. Deep learning analysis of the myocardium in coronary ct angiography for identification of patients with functionally significant coronary artery stenosis. *Medical image analysis*, 44:72–85, 2018.

[59] Franck Dernoncourt, Ji Young Lee, Ozlem Uzuner, and Peter Szolovits. De-identification of patient notes with recurrent neural networks. *Journal of the American Medical Informatics Association*, 24(3):596–606, 2017.

[60] Vasu Jindal, Javad Birjandtalab, M Baran Pouyan, and Mehrdad Nourani. An adaptive deep learning approach for ppg-based identification. In *2016 38th Annual international conference of the IEEE engineering in medicine and biology society (EMBC)*, pages 6401–6404. IEEE, 2016.

[61] Mirko Schiemann, Reinmar Killmann, Martin Kleen, Nasreddin Abolmaali, Jennifer Finney, and Thomas J Vogl. Vascular guide wire navigation with a magnetic guidance system: experimental results in a phantom. *Radiology*, 232(2):475–481, 2004.

[62] Walid Saliba, Jennifer E Cummings, Seil Oh, Youhua Zhang, Todor N Mazgalev, Robert A Schweikert, J David Burkhardt, and Andrea Natale. Novel robotic catheter remote control system: feasibility and safety of transseptal puncture and endocardial catheter navigation. *Journal of cardiovascular electrophysiology*, 17(10):1102–1105, 2006.

[63] Ejaz M Khan, William Frumkin, G Andre Ng, Suresh Neelagaru, Freddy M Abi-Samra, Jay Lee, and Giudici. First experience with a novel robotic remote

catheter system: Amigo™ mapping trial. *Journal of Interventional Cardiac Electrophysiology*, 37(2):121–129, 2013.

[64] Mitchell N Faddis, Walter Blume, Jennifer Finney, Andrew Hall, John Rauch, Jon Sell, Kyongtae Ty Bae, Michael Talcott, and Bruce Lindsay. Novel, magnetically guided catheter for endocardial mapping and radiofrequency catheter ablation. *Circulation*, 106(23):2980–2985, 2002.

[65] Allison M Okamura, Lawton N Verner, CE Reiley, and Mohsen Mahvash. Haptics for robot-assisted minimally invasive surgery. In *Robotics research*, pages 361–372. Springer, 2010.

[66] Mahta Khoshnam, Aaron Yurkewich, and Rajni V Patel. Model-based force control of a steerable ablation catheter with a custom-designed strain sensor. In *2013 IEEE International Conference on Robotics and Automation*, pages 4479–4484. IEEE, 2013.

[67] Bernhard Kübler, Ulrich Seibold, and Gerd Hirzinger. Development of actuated and sensor integrated forceps for minimally invasive robotic surger. *The International Journal of Medical Robotics and Computer Assisted Surgery*, 1(3):96–107, 2005.

[68] Wagahta Semere, Masaya Kitagawa, and Allison M Okamura. Teleoperation with sensor/actuator asymmetry: Task performance with partial force feedback. In *12th International Symposium on Haptic Interfaces for Virtual Environment and Teleoperator Systems, 2004. HAPTICS'04. Proceedings.*, pages 121–127. IEEE, 2004.

[69] Waqas Ullah, RJ Schilling, and T Wong. Contact force and atrial fibrillation ablation. *Journal of atrial fibrillation*, 8(5), 2016.

[70] Sterile single-use intravascular introducers, dilators and guidewires. *International Organization for Standardization, Geneva, Switzerland, Oct. 2014.*, 8(5), 2014.

[71] MK Konings, EB Van de Kraats, T Alderliesten, and WJ Niessen. Analytical guide wire motion algorithm for simulation of endovascular interventions. *Medical and Biological Engineering and Computing*, 41(6):689–700, 2003.

[72] Ahmed A Shabana. Flexible multibody dynamics: review of past and recent developments. *Multibody system dynamics*, 1(2):189–222, 1997.

[73] Tanja Alderliesten, Maurits K Konings, and Wiro J Niessen. Simulation of minimally invasive vascular interventions for training purposes. *Computer Aided Surgery*, 9(1-2):3–15, 2004.

[74] Jin Guo, Shuxiang Guo, Nan Xiao, and Baofeng Gao. Virtual reality simulators based on a novel robotic catheter operating system for training in minimally invasive surgery. *Journal of Robotics and Mechatronics*, 24(4):649, 2012.

[75] Mafalda Camara, Erik Mayer, Ara Darzi, and Philip Pratt. Soft tissue deformation for surgical simulation: a position-based dynamics approach. *International journal of computer assisted radiology and surgery*, 11(6):919–928, 2016.

[76] Shuai Li, Qing Xia, Aimin Hao, Hong Qin, and Qinping Zhao. Haptics-equiped interactive pci simulation for patient-specific surgery training and rehearsing. *Science China Information Sciences*, 59(10):103101, 2016.

[77] Julien Lenoir, Stephane Cotin, Christian Duriez, and Paul Neumann. Interactive physically-based simulation of catheter and guidewire. *Computers & Graphics*, 30(3):416–422, 2006.

[78] David B Camarillo, Christopher F Milne, Christopher R Carlson, Michael R Zinn, and J Kenneth Salisbury. Mechanics modeling of tendon-driven continuum manipulators. *IEEE transactions on robotics*, 24(6):1262–1273, 2008.

[79] Robert J Webster III and Bryan A Jones. Design and kinematic modeling of constant curvature continuum robots: A review. *The International Journal of Robotics Research*, 29(13):1661–1683, 2010.

[80] Mahta Khoshnam, Mahdi Azizian, and Rajni V Patel. Modeling of a steerable catheter based on beam theory. In *2012 IEEE International Conference on Robotics and Automation*, pages 4681–4686. IEEE, 2012.

[81] Larry L Howell, Spencer P Magleby, Brian Mark Olsen, and John Wiley. *Handbook of compliant mechanisms*. Wiley Online Library, 2013.

[82] Mahta Khoshnam and Rajni V Patel. Estimating contact force for steerable ablation catheters based on shape analysis. In *2014 IEEE/RSJ International Conference on Intelligent Robots and Systems*, pages 3509–3514. IEEE, 2014.

[83] Baofeng Gao, Shuxiang Guo, Nan Xiao, and Jin Guo. Design of the virtual reality based robotic catheter system for minimally invasive surgery training. In *2012 IEEE International Conference on Automation and Logistics*, pages 611–616. IEEE, 2012.

[84] Klaus-Jürgen Bathe and Said Bolourchi. Large displacement analysis of three-dimensional beam structures. *International journal for numerical methods in engineering*, 14(7):961–986, 1979.

[85] Matthias Hoffmann, Alexander Brost, Carolin Jakob, Martin Koch, Felix Bourier, Klaus Kurzidim, Joachim Hornegger, and Norbert Strobel. Reconstruction method for curvilinear structures from two views. In *Medical Imaging*

2013: Image-Guided Procedures, Robotic Interventions, and Modeling, volume 8671, page 86712F. International Society for Optics and Photonics, 2013.

[86] Hedyeh Rafii-Tari, Celia V Riga, Christopher J Payne, Mohamad S Hamady, Nicholas JW Cheshire, Colin D Bicknell, and Guang-Zhong Yang. Reducing contact forces in the arch and supra-aortic vessels using the magellan robot. *Journal of Vascular Surgery*, 64(5):1422–1432, 2016.

[87] Mohsen Moradi Dalvand, Saeid Nahavandi, and Robert D Howe. Fast vision-based catheter 3d reconstruction. *Physics in Medicine & Biology*, 61(14):5128, 2016.

[88] David B Dooner. Introducing radius of torsure and cylindroid of torsure. *Journal of Robotic Systems*, 20(8):429–436, 2003.

[89] Amir Hooshiar, Naghmeh M Bandari, and Javad Dargahi. Image-based estimation of contact forces on catheters for robot-assisted cardiovascular intervention. In *Proc. Hamlyn Symp. Med. Robot.*, pages 119–120, 2018.

[90] Carlos A Morillo, Atul Verma, Stuart J Connolly, Karl H Kuck, Girish M Nair, Jean Champagne, Laurence D Sterns, Heather Beresh, Jeffrey S Healey, and Andrea Natale. Radiofrequency ablation vs antiarrhythmic drugs as first-line treatment of paroxysmal atrial fibrillation (raaft-2): a randomized trial. *Jama*, 311(7):692–700, 2014.

[91] Carlo Bonanno, Mariemma Paccanaro, Luigi La Vecchia, Renato Ometto, and Alessandro Fontanelli. Efficacy and safety of catheter ablation versus antiarrhythmic drugs for atrial fibrillation: a meta-analysis of randomized trials. *Journal of Cardiovascular Medicine*, 11(6):408–418, 2010.

[92] Junghwan Back, Rashed Karim, Yohan Noh, Kawal Rhode, Kaspar Althoefer, and Hongbin Liu. Tension sensing for a linear actuated catheter robot. In

International Conference on Intelligent Robotics and Applications, pages 472–482. Springer, 2015.

[93] Vivek Muthurangu and Reza S Razavi. The value of magnetic resonance guided cardiac catheterisation, 2005.

[94] Luís Miguel Monteiro, Francisco Vasques-Nóvoa, Lino Ferreira, and Nascimento. Restoring heart function and electrical integrity: closing the circuit. *NPJ Regenerative medicine*, 2(1):1–13, 2017.

[95] Nilshan Ariyarathna, Saurabh Kumar, Stuart P Thomas, William G Stevenson, and Gregory F Michaud. Role of contact force sensing in catheter ablation of cardiac arrhythmias: evolution or history repeating itself? *JACC: Clinical Electrophysiology*, 4(6):707–723, 2018.

[96] Gregory Tholey, Jaydev P Desai, and Andres E Castellanos. Force feedback plays a significant role in minimally invasive surgery: results and analysis. *Annals of surgery*, 241(1):102, 2005.

[97] Sabine Ernst, Feifan Ouyang, Christian Linder, Klaus Hertting, Fabian Stahl, Julian Chun, Hitoshi Hachiya, Dietmar Bansch, Matthias Antz, and Karl-Heinz Kuck. Initial experience with remote catheter ablation using a novel magnetic navigation system: magnetic remote catheter ablation. *Circulation*, 109(12):1472–1475, 2004.

[98] János Radó, Csaba Dücső, Péter Földesy, Gábor Szebényi, Zbigniew Nawrat, Kamil Rohr, and Péter Fürjes. 3d force sensors for laparoscopic surgery tool. *Microsystem Technologies*, 24(1):519–525, 2018.

[99] Santhi Elayaperumal, Jung Hwa Bae, Bruce L Daniel, and Mark R Cutkosky. Detection of membrane puncture with haptic feedback using a tip-force sensing

needle. In *2014 IEEE/RSJ International Conference on Intelligent Robots and Systems*, pages 3975–3981. IEEE, 2014.

[100] Uikyum Kim, Yong Bum Kim, Dong-Yeop Seok, and Hyouk Ryeol Choi. S-surge: A portable surgical robot based on a novel mechanism with force-sensing capability for robotic surgery. In *Handbook of Robotic and Image-Guided Surgery*, pages 265–283. Elsevier, 2020.

[101] Lei Zhang, Feng Ju, Yanfei Cao, Yaoyao Wang, and Bai Chen. A tactile sensor for measuring hardness of soft tissue with applications to minimally invasive surgery. *Sensors and Actuators A: Physical*, 266:197–204, 2017.

[102] Naghmeh Bandari, Javad Dargahi, and Muthukumaran Packirisamy. Tactile sensors for minimally invasive surgery: A review of the state-of-the-art, applications, and perspectives. *IEEE Access*, 8:7682–7708, 2019.

[103] Sonia Pujol, Matthieu Pecher, Jean-Luc Magne, and Philippe Cinquin. A virtual reality based navigation system for endovascular surgery. *Studies in health technology and informatics*, pages 310–312, 2004.

[104] Matthias Gutberlet, Matthias Grothoff, Charlotte Eitel, Christian Lücke, Philip Sommer, Christopher Piorkowski, and Gerhard Hindricks. First clinical experience in man with the imricor-mr-ep system: Electrophysiology study guided by real-time mri. *Journal of Cardiovascular Magnetic Resonance*, 14(1):1–2, 2012.

[105] Karl-Heinz Kuck, Vivek Y Reddy, Boris Schmidt, Andrea Natale, Petr Neuzil, Nadir Saoudi, Josef Kautzner, and Herrera. A novel radiofrequency ablation catheter using contact force sensing: Toccata study. *Heart rhythm*, 9(1):18–23, 2012.

[106] Hoseok Song, Heechul Kim, Juwon Jeong, and Jungju Lee. Development of fbg sensor system for force-feedback in minimally invasive robotic surgery. In

2011 Fifth International Conference on Sensing Technology, pages 16–20. IEEE, 2011.

[107] Shahir Hasanzadeh and Farrokh Janabi-Sharifi. Model-based force estimation for intracardiac catheters. *IEEE/ASME Transactions on Mechatronics*, 21(1):154–162, 2015.

[108] Ryu Hwan-Taek, J. Woo, B. So, and B. Yi. Shape and contact force estimation of inserted flexible medical device. *International Journal of Control, Automation and Systems*, 18(1):163–174, 2020.

[109] John. A. Collins. Toward image data-driven predictive modeling for guiding thermal ablative therapy. *IEEE Transactions on Biomedical Engineering*, 67(6):1548–1557, 2019.

[110] Mohammad Jolaei, Amir Hooshiar, and Javad Dargahi. Displacement-based model for estimation of contact force between rfa catheter and atrial tissue with ex-vivo validation. In *2019 IEEE International Symposium on Robotic and Sensors Environments (ROSE)*, pages 1–7. IEEE, 2019.

[111] Mahta Khoshnam, Allan C Skanes, and Rajni V Patel. Modeling and estimation of tip contact force for steerable ablation catheters. *IEEE Transactions on Biomedical Engineering*, 62(5):1404–1415, 2015.

[112] Masoud Razban, Javad Dargahi, and Benoit Boulet. A sensor-less catheter contact force estimation approach in endovascular intervention procedures. In *2018 IEEE/RSJ International Conference on Intelligent Robots and Systems (IROS)*, pages 2100–2106. IEEE, 2018.

[113] Junghwan Back, Lukas Lindenroth, Rashed Karim, Kaspar Althoefer, Kawal Rhode, and Hongbin Liu. New kinematic multi-section model for catheter contact force estimation and steering. In *2016 IEEE/RSJ International Conference on Intelligent Robots and Systems (IROS)*, pages 2122–2127. IEEE, 2016.

[114] Nils Gessert, Torben Priegnitz, Thore Saathoff, Sven-Thomas Antoni, David Meyer, Moritz Franz Hamann, Klaus-Peter Jünemann, Christoph Otte, and Alexander Schlaefer. Needle tip force estimation using an oct fiber and a fused convgru-cnn architecture. In *International conference on medical image computing and computer-assisted intervention*, pages 222–229. Springer, 2018.

[115] Angelica I Aviles. Exploring the effects of dimensionality reduction in deep networks for force estimation in robotic-assisted surgery. In *Medical Imaging 2016: Image-Guided Procedures, Robotic Interventions, and Modeling*, volume 9786, page 97861X. International Society for Optics and Photonics, 2016.

[116] Ali Tavakoli Golpaygani, Siamak Najarian, and Mehdi Movahedi. Tactile sensor for robotic applications. In *World Congress on Medical Physics and Biomedical Engineering, September 7-12, 2009, Munich, Germany*, pages 2299–2302. Springer, 2009.

[117] Mohammad A Qasaimeh, S Sokhanvar, J Dargahi, and M Kahrizi. A micro-tactile sensor for in situ tissue characterization in minimally invasive surgery. *Biomedical microdevices*, 10(6):823–837, 2008.

[118] Feng Ju, Yaming Wang, Zhao Zhang, Yaoyao Wang, Yahui Yun, Hao Guo, and Bai Chen. A miniature piezoelectric spiral tactile sensor for tissue hardness palpation with catheter robot in minimally invasive surgery. *Smart Materials and Structures*, 28(2):025033, 2019.

[119] Jung-Hoon Hwang, Joon Ho Kwon, Tae-Keun Kim, and Daehie Hong. Design of simple structured tactile sensor for the minimally invasive robotic palpation. In *2013 IEEE/ASME International Conference on Advanced Intelligent Mechatronics*, pages 1296–1299. IEEE, 2013.

[120] Masoud Kalantari and Ramezanifard. A piezoresistive tactile sensor for tissue characterization during catheter-based cardiac surgery. *The International Journal of Medical Robotics and Computer Assisted Surgery*, 7(4):431–440, 2011.

[121] Panagiotis Polygerinos and Schaeffter. A fibre-optic catheter-tip force sensor with mri compatibility: A feasibility study. In *2009 Annual International Conference of the IEEE Engineering in Medicine and Biology Society*, pages 1501–1054. IEEE, 2009.

[122] Katsuaki Yokoyama. Novel contact force sensor incorporated in irrigated radiofrequency ablation catheter predicts lesion size and incidence of steam pop and thrombus. *Circulation: Arrhythmia and Electrophysiology*, 1(5):354–362, 2008.

[123] Tohyama, M Kohashi, M Sugihara, and H Itoh. A fiber-optic pressure microsensor for biomedical applications. *Sensors and Actuators A: Physical*, 66(1-3):150–154, 1998.

[124] Junghwan Back, Lukas Lindenroth, Kawal Rhode, and Hongbin Liu. Three dimensional force estimation for steerable catheters through bi-point tracking. *Sensors and Actuators A: Physical*, 279:404–415, 2018.

[125] Jiayin Cai, Hongzhi Xie, Shuyang Zhang, and Lixu Gu. Blood flow-induced physically based guidewire simulation for vascular intervention training. *International Journal of Computer Assisted Radiology and Surgery*, 12(9):1571–1583, 2017.

[126] Shuxiang Guo, Miao Yu, Yu Song, and Linshuai Zhang. The virtual reality simulator-based catheter training system with haptic feedback. In *2017 IEEE International Conference on Mechatronics and Automation (ICMA)*, pages 922–926. IEEE, 2017.

[127] Haoyu Wang. A robust and fast approach to simulating the behavior of guidewire in vascular interventional radiology. *Computerized Medical Imaging and Graphics*, 40:160–169, 2015.

[128] Vladimir Vapnik and Vlamimir Vapnik. Statistical learning theory wiley. *New York*, 1:624, 1998.

[129] Joarder Kamruzzaman, Ruhul A Sarker, and Iftekhar Ahmad. Svm based models for predicting foreign currency exchange rates. In *Third IEEE International Conference on Data Mining*, pages 557–560. IEEE, 2003.

[130] AJ Smola and B Schölkopf. A tutorial on support vector regression, ntr nc-tr-98-030, editor. 1998.

[131] Véronique L Roger, Alan S Go, Donald M Lloyd-Jones, Emelia J Benjamin, and Berry. Heart disease and stroke statistics—2012 update: a report from the american heart association. *Circulation*, 125(1):e2, 2012.

[132] Valentin Fuster and Ryd. A report of the american college of cardiology/american heart association task force on practice guidelines and the european society of cardiology committee for practice guidelines. *Circulation*, 114(7):e257–e354, 2006.

[133] Mark A Wood, Chris Brown-Mahoney, G Neal Kay, and Kenneth A Ellenbogen. Clinical outcomes after ablation and pacing therapy for atrial fibrillation: a meta-analysis. *Circulation*, 101(10):1138–1144, 2000.

[134] Allison . M. Okamura. Haptic feedback in robot-assisted minimally invasive surgery. *Current opinion in urology*, 19(1):102, 2009.

[135] H. Xin, J.S. Zelek, and H. Carnahan. Laparoscopic surgery, perceptual limitations and force: A review. In *First Canadian student conference on biomedical computing*, volume 144, 2006.

[136] Nabil Zemiti, Guillaume Morel, Tobias Ortmaier, and Nicolas Bonnet. Mechatronic design of a new robot for force control in minimally invasive surgery. *IEEE/ASME Transactions On Mechatronics*, 12(2):143–153, 2007.

[137] Masaya. Kitagawa, D. Dokko, A.M. Okamura, and D. Yuh. Effect of sensory substitution on suture-manipulation forces for robotic surgical systems. *The Journal of thoracic and cardiovascular surgery*, 129(1):151–158, 2005.

[138] Allison . M. Okamura. Methods for haptic feedback in teleoperated robot-assisted surgery. *Industrial Robot: An International Journal*, 2004.

[139] Ryan . E. Schoonmaker and Caroline GL. Cao. Vibrotactile force feedback system for minimally invasive surgical procedures. In *2006 IEEE international conference on systems, man and cybernetics*, volume 3, pages 2464–2469. IEEE, 2006.

[140] Javad. Dargahi, M. Parameswaran, and S. Payandeh. A micromachined piezoelectric tactile sensor for an endoscopic grasper-theory, fabrication and experiments. *Journal of microelectromechanical systems*, 9(3):329–335, 2000.

[141] Daniel. Pawluk. A distributed pressure sensor for biomechanical measurements. *J BIOMECH ENG TRANS ASME*, 120(2):302–305, 1998.

[142] Hoseok. Song, Heechul . Kim, J. Jeong, and j. Lee. Development of fbg sensor system for force-feedback in minimally invasive robotic surgery. In *2011 Fifth International Conference on Sensing Technology*, pages 16–20, 2011.

[143] Shahir. Hasanzadeh and F. Janabi-Sharifi. Model-based force estimation for intracardiac catheters. *IEEE/ASME Transactions on Mechatronics*, 21(1):154–162, 2016.

[144] Shaoqing. Ren, K. He, R. Girshick, and J. Sun. Faster r-cnn: Towards real-time object detection with region proposal networks. *IEEE Transactions on Pattern Analysis and Machine Intelligence*, 39(6):1137–1149, 2017.

[145] Chien-Yao. Wang Alexey. Bochkovskiy and H. M. Liao. Yolov4: Optimal speed and accuracy of object detection, 2020.

[146] Jean. Deng. ImageNet: A Large-Scale Hierarchical Image Database. In *CVPR09*, 2009.

[147] Alex. Krizhevsky, I. Sutskever, and G. E. Hinton. Imagenet classification with deep convolutional neural networks. In *Proceedings of the 25th International Conference on Neural Information Processing Systems - Volume 1*, NIPS'12, page 1097–1105, Red Hook, NY, USA, 2012. Curran Associates Inc.

[148] Martin. Abadi. TensorFlow: Large-scale machine learning on heterogeneous systems, 2015. Software available from tensorflow.org.